2017

Projecting regional climate and cropland changes using a linked biogeophysical-socioeconomic modeling framework: 1 Model description and an equilibrium application over West Africa

Guiling Wang

Kazi Farzan Ahmed

Liangzhi You

Miao Yu

Jeremy S. Pal
Loyola Marymount University, jpal@lmu.edu

See next page for additional authors

AGU PUBLICATIONS

Journal of Advances in Modeling Earth Systems

RESEARCH ARTICLE
10.1002/2016MS000712

This article is a companion to *Ahmed et al.* [2017], doi:10.1002/2016MS000721.

Key Points:
- Yield for most crops in West Africa would decrease in the future despite some projected increase of precipitation
- The dominant driver for future cropland expansion in West Africa would be yield decrease in the west and food demand increase in the east
- The projected expansion of cropland enhances a dry(west)-wet(east) dipole pattern of precipitation changes caused by CO_2 changes

Correspondence to:
G. Wang,
guiling.wang@uconn.edu;
L. You,
youliangzhi@caas.cn

Citation:
Wang, G., K. F. Ahmed, L. You, M. Yu, J. Pal, and Z. Ji (2017), Projecting regional climate and cropland changes using a linked biogeophysical-socioeconomic modeling framework: 1. Model description and an equilibrium application over West Africa, *J. Adv. Model. Earth Syst.*, *9*, 354–376, doi:10.1002/2016MS000712.

Received 11 MAY 2016
Accepted 22 DEC 2016
Accepted article online 7 JAN 2017
Published online 7 FEB 2017

Projecting regional climate and cropland changes using a linked biogeophysical-socioeconomic modeling framework: 1. Model description and an equilibrium application over West Africa

Guiling Wang[1], Kazi Farzan Ahmed[1], Liangzhi You[2,3], Miao Yu[1,4], Jeremy Pal[5], and Zhenming Ji[1,5]

[1]Department of Civil and Environmental Engineering, University of Connecticut, Storrs, Connecticut, USA, [2]Key Laboratory of Agri-informatics, Ministry of Agriculture/Institute of Agricultural Resources and Regional Planning, Chinese Academy of Agricultural Sciences, Beijing, China, [3]International Food Policy Research Institute, Washington, District of Columbia, USA, [4]Collaborative Innovation Center on Forecast and Evaluation of Meteorological Disasters/Key Laboratory of Meteorological Disaster of Ministry of Education, Nanjing University of Information Science and Technology, Nanjing, China, [5]Department of Civil Engineering and Environmental Science, Loyola Marymount University, Los Angeles, California, USA

Abstract Agricultural land use alters regional climate through modifying the surface mass, energy, and momentum fluxes; climate influences agricultural land use through their impact on crop yields. These interactions are not well understood and have not been adequately considered in climate projections. This study tackles the critical linkages within the coupled natural-human system of West Africa in a changing climate based on an equilibrium application of a modeling framework that asynchronously couples models of regional climate, crop yield, multimarket agricultural economics, and cropland expansion. Using this regional modeling framework driven with two global climate models, we assess the contributions of land use change (LUC) and greenhouse gas (GHGs) concentration changes to regional climate changes and assess the contribution of climate change and socioeconomic factors to agricultural land use changes. For future cropland expansion in West Africa, our results suggest that socioeconomic development would be the dominant driver in the east (where current cropland coverage is already high) and climate changes would be the primary driver in the west (where future yield drop is severe). For future climate, it is found that agricultural expansion would cause a dry signal in the west and a wet signal in the east downwind, with an east-west contrast similar to the GHG-induced changes. Over a substantial portion of West Africa, the strength of the LUC-induced climate signals is comparable to the GHG-induced changes. Uncertainties originating from the driving global models are small; human decision making related to land use and international trade is a major source of uncertainty.

1. Introduction

Prediction of future climate is more than just prediction of greenhouse gas (GHG) emissions and their resulting climatic response. Land cover changes of both natural and anthropogenic origins pose another significant forcing for regional and global climates, through their impact on surface albedo, Bowen ratio, surface roughness, and aerosol emission [e.g., *Feddema et al.*, 2005a; *Lawrence et al.*, 2011; *Yu et al.*, 2015; *Wang et al.*, 2016]. In the past decade, model development efforts worldwide have led to the incorporation of natural vegetation dynamics (as represented by dynamic global vegetation models of various type and complexity, e.g., *Kucharik et al.* [2000], *Cox* [2001], *Bonan et al.* [2003], and *Sitch et al.* [2003]) into several regional and global climate models [see *Wang et al.*, 2015, and the reviews therein]. Some of these models participated in the Coupled Model Intercomparison Project phase 5 (CMIP5), providing future climate projections that account for the impact of naturally induced vegetation cover changes [e.g., *Bonan and Levis*, 2006; *Gent et al.*, 2011; *Collins et al.*, 2011; *Dunne et al.*, 2012]. However, land cover changes of anthropogenic origin such as agricultural land use changes [e.g., *Hurtt et al.*, 2011] were either not accounted for or treated as an external forcing in CMIP5. In the latter case, land use changes were projected primarily based on socioeconomic development and then provided to climate models as an input forcing, which does not allow for

interactions between land use and climate changes. This study attempts to fill this research gap, projecting future climate and agricultural land use changes accounting for the coupled dynamics between the natural and human systems.

The primary drivers for agricultural land use are population change and other socioeconomic developments such as agricultural technology changes, food policies, international trade, and changes of dietary preferences. Naturally, most previous modeling and predictions of agricultural land use were primarily socioeconomically driven [e.g., *Agarwal et al*., 2002; *Parker et al*., 2002; *Verburg et al*., 2006; *Schaldach et al*., 2011; *Schmitz et al*., 2014]. Recently, climate change has become an increasingly important stressor for agricultural systems across the globe, posing a grant challenge for the world food security. Global climate influences regional agriculture through its impact on global crop production therefore international trade and world crop price; regional climate influences agriculture though its direct impact on farming systems, agricultural water management, and agricultural productivity. As the agricultural system (including farmers and policy makers) responds and adapts to these changes, climate is becoming an important biophysical driver shaping land use and land cover changes in agricultural regimes, which then feedback to further influence regional climate. While agroeconomics models have started to incorporate the impact of climate change on crop suitability [e.g., *Schmitz et al*., 2014], the impact of climate changes on land use has not been accounted for in the current generation of earth system models. This omission is a potentially important source of uncertainty in future projections. Since land use influences both economic development and regional climate, it is desirable to combine climate changes, land use changes, and other socioeconomic drivers into one modeling framework used for future projections. This is especially critical for regions like West Africa where climate is sensitive to land cover changes, agriculture is a major livelihood in almost all the countries, and food production is already stressed by climate.

West Africa is well known for its climate sensitivity to land use land cover changes, as is evident from a considerable body of literature on modeling the impact of prescribed land use changes [e.g., *Xue and Shukla*, 1993; *Abiodun et al*., 2008; *Wang et al*., 2016] and natural vegetation dynamics [e.g., *Zeng et al*., 1999; *Wang et al*., 2004; *Delire et al*., 2004, 2011; *Alo and Wang*, 2010; *Yu et al*., 2015; *Erfanian et al*., 2016]. Land use land cover changes influence regional climate primarily through modifying land surface properties (e.g., surface albedo, Bowen ratio, and roughness) that control the land-atmosphere mass, energy, and momentum exchanges. The impact of these changes depends on the scale and nature of land cover changes [*Moorcroft*, 2003; *Lawrence and Vandecar*, 2014]. At smaller scales, land cover changes such as deforestation enhance the surface heterogeneity, leading to the development of mesoscale circulations with rising motion over warmer (deforested) areas. This could enhance convection, cloudiness, and even precipitation over deforested areas [e.g., *Wang et al*., 2000, 2009; *Baidya Roy and Avissar*, 2002]. At large scales in the Tropics, land cover degradation (e.g., from forest to cropland or from grassland to bare soil) tends to cause drying and warming in the rainy season and cooling in the dry season [*Xue and Shukla*, 1993; *Wang et al*., 2016]. Decrease of rainfall could result from a decrease in surface net radiation (due to an albedo increase) that suppresses convection, a decrease in evapotranspiration that limits local moisture supply for precipitation, and changes in large-scale circulation that reduces atmospheric moisture flux convergence [*Wang et al*., 2016]. The decrease in evaporative cooling in the wet Tropics tends to dominate over the albedo effect in the wet season, leading to a net warming effect. Land use and land cover have gone through major changes in the past century [*Ramankutty et al*., 2008; *Monfreda et al*., 2008], and were projected to continue to change in the future, globally, and in Africa in particular [*Hurtt et al*., 2011; *Yu et al*., 2014; *Schmitz et al*., 2014; *Ahmed et al*., 2016]. At the global scale, land use changes were projected to modify the predicted future climate, with enhancing effects in some regions and dampening effects in others [e.g., *Feddema et al*., 2005b; *Ramankutty et al*., 2006; *Davies-Barnard et al*., 2014a, 2014b; *Jones et al*., 2015]. Regionally in West Africa, historical land use was found to contribute to the development of the Sahel drought in the second half of the twentieth century [e.g., *Hagos et al*., 2014; *Wang et al*., 2016]. It is critical that future projections of regional climate change account for the impact of future land use changes.

In most of West Africa, crop production is primarily rain fed, and agricultural development is constrained by both heat and water stresses. Warming in a future climate will exacerbate the crop heat stress, and also accelerate evapotranspiration which then further reduces moisture availability in the soil and shortens the suitable growing season [*Cook and Vizy*, 2013]. Therefore, future climate changes in this region are likely to cause a reduction of crop yield despite the CO_2 fertilization effects and potential increase of precipitation in

some areas [*Schlenker and Lobell*, 2010; *Lobell et al*., 2011; *Ruane et al*., 2013; *Waha et al*., 2013; *Sultan et al*., 2013; *Ahmed et al*., 2015]. The climate-induced decline of agricultural productivity together with population increase presents a constant pressure for agricultural expansion and intensification. Africa's agricultural productivity is the lowest in the world, which leaves sufficient room for intensification and improvement. However, more than 80% of Africa's agricultural output growth since 1980 has come from the expansion of cropland areas, rather than from greater productivity of areas already cultivated [*Rosegrant et al*., 2011]. Among the various options for agricultural intensification in West Africa, irrigation has the greatest potential [*Svendsen et al*., 2009; *You et al*., 2009; *Xie et al*., 2014]. However, as irrigation requires infrastructure that has a long planning and construction period, widespread practice of irrigation is therefore not feasible in the near term. In fact, most studies assessing future climate impact on crop yield assumed rain-fed agriculture [e.g., *Asseng et al*., 2013; *Ahmed et al*., 2015]. Due to the lack of effective options for intensification, agriculture expansion will be the primary strategy to combat the climate-induced food shortage in the foreseeable future. Projections for future land use need to account for the impact of climate changes.

Assuming that agricultural land use practices will be informed of and respond to projected climate change impacts, this study tackles whether and by how much including climate-land use interactions in predictive models might influence future projected changes in climate and cropland expansion in West Africa. Based on a modeling framework that accounts for both the biophysical and socioeconomic drivers for cropland expansion and the feedback of land cover changes on regional climate, this study attempts (1) to assess future climate change and cropland expansion in West Africa considering the interaction between climate and land use, (2) to compare the effects of GHG concentration changes and cropland expansion on regional climate changes, and (3) to compare the effects of climate change and socioeconomic development on cropland expansion. In this study, our projection of the future is limited to the midcentury, and the CO_2 concentration from the Representative Concentration Pathway (RCP) 8.5 is used as the climate change driver. Despite differences among different RCP scenarios, they remain small before midcentury [*IPCC*, 2013].

2. Models Description

This study makes use of a modeling framework that accounts for the impact of GHG-induced climate changes, socioeconomic development, response of cropland allocation to yield changes, and impact of land cover changes on regional climate. The modeling framework includes a cascade of four different models (Figure 1), each serving a distinct purpose: (1) a Regional Climate Model coupled with an updated land surface model (RegCM4.3.4-CLM4.5) [*Wang et al*., 2015], which simulates and predicts the regional climate driven with boundary conditions from coarse resolution GCMs; (2) a crop modeling system (DSSAT) [*Hoogenboom et al*., 2012], which includes three different types of crop growth models, each applicable for evaluating the productivity of a specific set of crops under any given climate; (3) a partial equilibrium economic model (IMPACT) [*Rosegrant*, 2012], which provides (among many other outputs) estimate of demands for crops based on socioeconomic drivers and accounts for international trade of agricultural commodities; (4) a cropland projection model (LandPro_Crop) [*Ahmed et al*., 2016], which prioritizes allocation of available land to different crop types based on existing land use, future crop yield, and future demand for crops. These four models are asynchronously coupled. As shown in Figure 1, both the Regional Climate Model RegCM4.3.4-CLM4.5 ("RCM" hereafter) and the economic model IMPACT are driven by output from global models; the RCM produces the meteorological forcing needed by the crop model DSSAT; DSSAT simulates crop yield while IMPACT estimates the

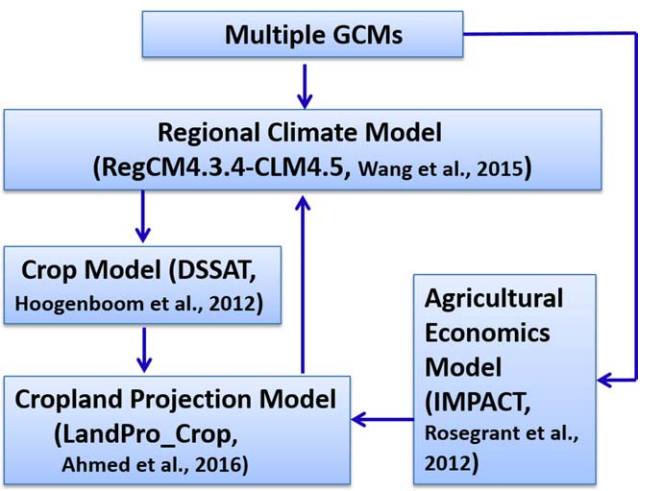

Figure 1. Diagram of the asynchronously coupled modeling framework.

effective food demands, both of which are inputs to the cropland projection model LandPro_Crop, which produces updated land use land cover map for the RCM. The four models are briefly introduced in the following.

2.1. RegCM4.3.4-CLM4.5 and Performance

The regional climate system model results from the synchronous coupling of two major models: the Abdus Salam International Centre for Theoretical Physics (ICTP) Regional Climate Model (RegCM) version 4.3.4 [*Giorgi et al*., 2012], and a modified version of the Community Land Model (CLM) that performs similarly to CLM4.5 [*Oleson et al*., 2013; *Yu et al.*, 2014]. Details of the model development and validation over Tropical Africa can be found in *Wang et al*. [2015].

RegCM4.3.4 is a limited-area model simulating atmospheric physics and dynamics, using a terrain-following σ-pressure vertical coordinate system and an Arakawa B-grid finite differencing algorithm. The model includes a hydrostatic dynamical core [*Grell et al*., 1994], an atmospheric radiation scheme [*Kiehl et al*., 1996], an aerosols scheme [*Solmon et al*., 2006; *Zakey et al*., 2006], a nonlocal boundary layer scheme [*Holtslag et al*., 1990], a large-scale cloud and precipitation scheme [*Pal et al*., 2000], and multiple options for convection parameterizations. Based on sensitivity tests over the West Africa domain, when coupled with the land surface model CLM4.5, the Emanuel convection scheme [*Emanuel*, 1991] performs the best for this region and is chosen for this study.

CLM4.5 solves the surface hydrological and biogeophysical processes and uses a hierarchical data structure to represent land surface heterogeneity. Multiple land units (e.g., glacier, lake, wetland, urban, vegetated land, and their further delineations) can coexist in each grid cell, multiple soil/snow columns can coexist in each land unit, and multiple plant functional types (PFTs) can coexist on each column of vegetated land. Vegetation is represented by a combination of different PFTs that differ in physiology and structure and include both crops and natural vegetation. In the vertical direction, each column can include 15 soil layers and up to 5 snow layers. Soil and snow state variables are defined at the column level, and all vegetation variables are defined at the PFT level. Calculations for surface mass and energy fluxes within a vegetated land unit take place at the PFT level, and the area-weighted average of the surface fluxes from different components (PFTs, columns, and land units) within each grid cell is passed to RegCM4.3.4.

CLM4.5 includes optional submodels for surface biogeochemical processes, vegetation phenology, and vegetation dynamics. Depending on which are chosen, the distribution, density, structure, and phenology of the PFTs can be either prescribed or predicted by the model. As the focus of this study is on agricultural land use and its interaction with regional climate, the leaf area index (LAI), LAI seasonality, and spatial coverage of each PFT in the present-day simulations are prescribed based on the data of *Lawrence and Chase* [2007] and *Lawrence et al.* [2011] to exclude the uncertainties related to natural vegetation dynamics. As the projection progresses into the future, agricultural land use will expand and some natural PFTs will be converted to crops. The resulting temporally evolving PFTs spatial coverage will be used by each of the RegCM4.3.4-CLM4.5 future runs to account for the anthropogenic land cover changes.

As a Regional Climate Model, RegCM4.3.4-CLM4.5 requires initial and boundary conditions (ICBCs) that can be derived from either reanalysis data or global models. The performance of the model in simulating the present-day climate of West Africa has been documented based on simulations driven with ICBCs from the ECMWF ERA-Interim data [*Wang et al*., 2015] and from multiple global models including MIROC-ESM and CCSM4 version of CESM [*Yu et al*., 2015; *Ji et al*., 2016, 2017]. The same model configuration and same resolutions are used here over the same spatial domain. The spatial resolution is 50 km horizontally with 18 vertical layers, and the time step is 100 seconds. Using precipitation during the monsoon season (June-July-August-September, JJAS) as an example, Figure 2 presents the model present-day climate and biases relative to the University of Delaware (UDel) precipitation data. For the model driven with ERA-Interim data, the center of the tropical rain belt is located slightly too far north, leading to a general overestimation in the Sahel and slight underestimation along the Guinea Coast. When driven with ICBCs from the CESM or MIROC-ESM historical runs, the model simulates a tropical rain belt that does not penetrate northward enough, with a general underestimation in the Sahel and overestimation along the Guinea Coast. The overestimation along the Guinea Coast is especially pronounced in the MIROC-ESM-driven simulation. In all three simulations, the rain belt is narrower and more concentrated than in the UDel data, which leads to an underestimation of rainfall along the edges of the rain belt (with a large magnitude of relative bias near the desert due to the small magnitude

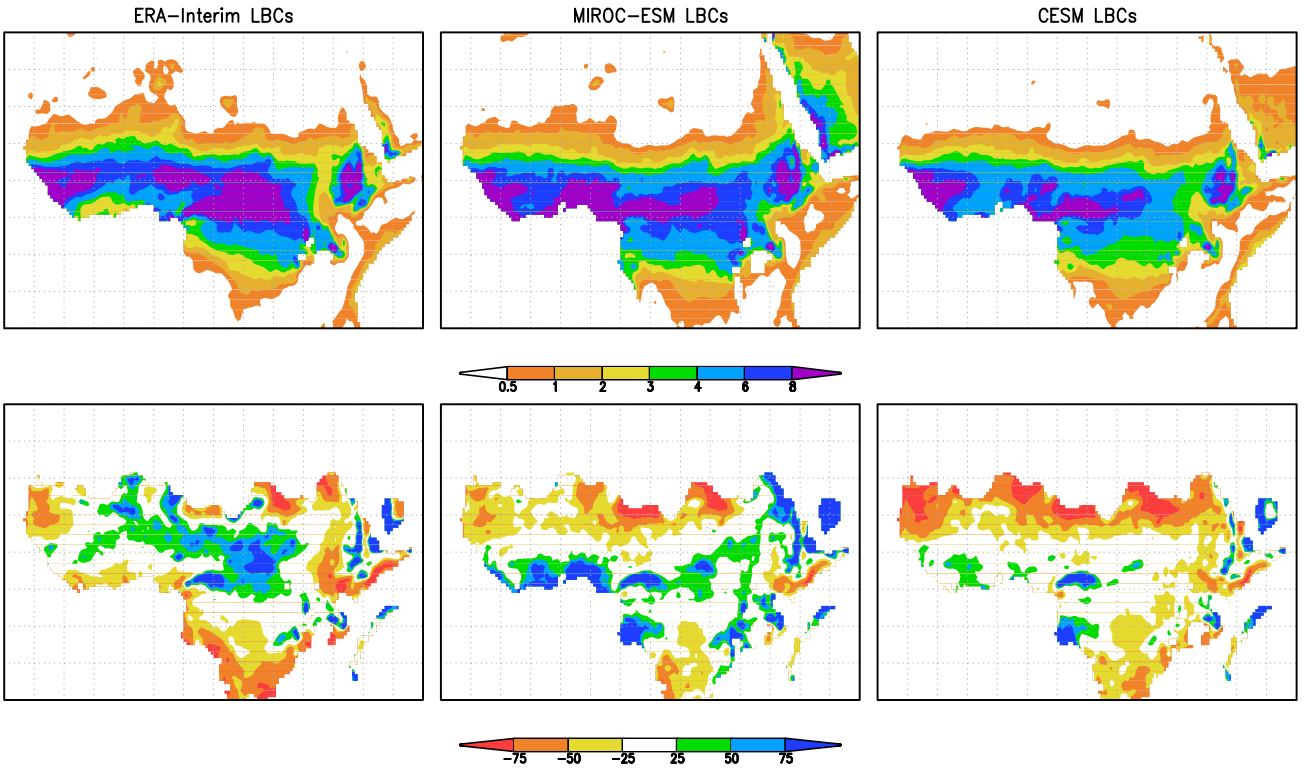

Figure 2. (top) Mean JJAS precipitation (in mm/d) during 1981–2000 simulated by RegCM4.3.4-CLM4.5 driven with ICBCs (left) from the ERA-Interim data, (middle) from the MIROC-ESM, and (right) from CESM; (bottom) the corresponding model biases relative to the University of Delaware data (in %).

of the observed precipitation used to normalize the model bias). Compared with the UDel surface air temperature data, the RCM bias driven with all ICBCs in JJAS is within 1°C over the sub-Saharan Africa (results not shown). The largest bias for temperature is an underestimation over the Sahara Desert by as much as 5°C.

2.2. DSSAT and Calibration

The Decision Support System for Agrotechnology Transfer (DSSAT) is a software package combining soil and weather databases with crop models and application programs to simulate multiyear outcomes of crop management strategies [*Jones et al.*, 2003]. DSSAT version 4.5 [*Hoogenboom et al.*, 2012] is used in this study. While DSSAT can be useful for many other purposes, in this study we are interested mainly in its cropping system model for crop yield. There are three main crop growth modules, each dealing with a different set of crops: CROPGRO [*Boote et al.*, 1998] for grain legumes (e.g., soybean and peanut), CERES [*Ritchie et al.*, 1998] for grain cereals (e.g., rice, maize, and millet), and SUBSTOR [*Ritchie et al.*, 1995] for root crops (e.g., cassava and potato). These models simulate daily increment of plant biomass taking into account of plant genetics, daily weather conditions, soil properties and management factors. For example, in the CERES module of DSSAT, seven stages of the plant life cycle are considered: germination, emergence, end of juvenile, floral induction, flowering, beginning of grain fill, and physiological maturity. The growing degree days (GDD) is used to determine the rate of development, and the GDDs required for the transition between two successive growth stages are cultivar specific. To calculate the daily growth rate, crop-specific ecotype coefficient for radiation use efficiency is used to convert the daily intercepted photosynthetically active radiation to plant dry matter. Grain filling in cereal plants is regulated by the cultivar's genetic potential, rate of carbohydrate accumulation during flowering, temperature, water stress, and available nitrogen.

In the application to West Africa, we consider five major crops: maize, millet, sorghum, peanut, and cassava. These crops are important sources of calories and nutrition in West African countries, and are among the top major crops based on total area harvested and their economic values in the region [*You et al.*, 2009]. According to data from *FAO et al.* [2006], these five crops account for approximately 80% of the total harvested area in West Africa. All five crops are primarily rain fed in West Africa, and cultivars common in the region are chosen for DSSAT to simulate. These include the Obatampa cultivar for maize with a growing

season length of ~90 days, the CSM 335 cultivar for sorghum with a growing season of ~110 days, the CIVT cultivar for millet with a growing season length of 85 days, the Chinese cultivar for peanut with a growing season of 100–110 days, and the MCol22 cultivar for cassava with a harvest date set one year after planting (based on current practice in West Africa).

We ran DSSAT at a spatial scale of 0.5° for the West African region. However, as grid-level observational data for crop harvest yield are either sparse or not available at all, in this study, we use the FAO country-average yearly yield data for individual crops (FAOSTAT database) as the observational reference to guide the DSSAT model calibration. So the model is calibrated at the country level, and for each crop and each country independently. This is accomplished by adjusting the fertilizer input and planting month for each individual crop within each country in order to match the DSSAT country-average yield with the FAO data based on the long-term mean during 1980–1998. Calibration has been conducted for 13 countries in West Africa, including Benin, Burkina Faso, Gambia, Ghana, Guinea, Guinea-Bissau, Ivory Coast, Mali, Niger, Nigeria, Senegal, Sierra Leone, and Togo. One West African country, Liberia, is excluded due to the lack of reliable data for crop yield during the civil wars. The calibrated model input parameters, including the cultivar, per hectare fertilizer applications for each crop in each country, and planting month (which allows for adjustment of planting date within a certain range according to soil moisture conditions) are used for the DSSAT future projection runs, assuming that the present-day common practice of crop management will continue into the future. Among these parameters, crop yield in West Africa is most sensitive to the amount of fertilizers applied. In the absence of irrigation, increasing fertilizer input would likely be the most effective strategy for agricultural intensification in this region and therefore an important source of uncertainty for future projections.

Running DSSAT requires several ancillary data, including the International Soil Reference and Information Center (ISRIC)'s reanalyzed World Inventory of Soil Emission Potentials (WISE) soil database version 1.1 (*Batjes* [2002] and *Romero* [2012], which includes 3404 valid soil profiles across the globe), the geographically explicit N and P fertilizer application data set [*Potter et al*., 2010] at 0.5° spatial resolution, and the global manure distribution data at 0.5° resolution [*Wint and Robinson*, 2007]. For the planting time data, we followed the FAO crop calendar [*IIASA/FAO*, 2012] that selects the local onset of monsoon rainfall as the planting period for rain-fed crops. Specifically, a planting month is chosen based on the typical monsoon onset time; the model then determines the planting date based on the time when soil moisture reaches a specified threshold within the planting month. Therefore, the planting date is not strictly prescribed. Instead, it varies within a certain range depending on climate. Further details can be found in *Ahmed et al.* [2015].

2.3. IMPACT

The International Model for Policy Analysis of Agricultural Commodities and Trade (IMPACT) was developed in the 1990s to support food policy analysis [*Rosegrant et al*., 1995], and has been used as a tool to analyze the effects of population, investment, and trade scenarios on food security. The model has been continuously improved, and the latest version [*Rosegrant*, 2012] is used in this study. The model is considered a leading agricultural sector model within the global agricultural policy research community. In this study, IMPACT is used to estimate the demand for various crops considering international trade (through which part of the demand for food in import countries is met by nonlocal production and part of the production in export countries is used to meet nonlocal demand).

IMPACT is a partial equilibrium, global agricultural sector model representing a competitive agricultural market for crops and livestock. This multimarket model simulates the operation of national and international markets, solving for production, demand, and prices that equate supply and demand across the globe. Within each country or subnational region, supplies, demands, and prices for all agricultural commodities are determined; all country and regional agricultural submodels are linked through trade. World agricultural commodity prices are determined annually at levels that clear international markets. Domestic prices are a function of world prices, adjusted by the effect of price policies (such as taxation or subsidy borne by producers or consumers relative to world prices) and other factors such as transport and marketing costs.

Domestic demand for a commodity is the sum of its demand for food and feed. Food demand is a function of the price of the commodity and the prices of other competing commodities, per capita income, and total population. Per capita income and population increase annually according to country-specific population and income growth rates derived based on socioeconomic data. Feed demand is a derived demand

determined by the changes in livestock production, feed ratios, and own- and cross-price effects of feed crops. A large set of census and ground-based data are used to set the parameters in the model.

IMPACT can be run over a specific region or over the globe, and was run over the globe in this study. To project the future, here IMPACT was run under the Shared Socioeconomic Pathway-2 (SSP2) that is characterized by an economic development pattern following historical trends and medium population growth. The future climate forcing used to drive IMPACT was derived from the RCP8.5 experiments of CMIP5 models, consistent with the scenario used for the regional climate modeling in section 2.1. To reduce the climate model-related uncertainties, four IMPACT runs were conducted, each driven with global climate output from GFDL-ESM2M, HadGEM2-ES, IPSL-CM5A-LR, and MIROC-ESM, respectively, and the average of output from the four IMPACT runs was used in this study. For each country of the world, IMPACT projects the future scenarios of supply, demand and price for more than 40 food commodities. For each country in West Africa and each commodity, of the many outputs from IMPACT, future scenarios for total domestic demand and effective demand (i.e., "domestic demand minus imports" or "domestic demand plus exports") are used here as inputs to the cropland projection model (described in section 2.4). Most countries in West Africa are food import countries, with effective demand lower than total demand.

2.4. LandPro_Crop

Socioeconomic factors are the main driver for land use changes in a stationary climate. To project land use in a changing climate, it is important to also account for the impact of future climate change, which influences cropland expansion through its impact on crop yield and on human decision making in adapting to the climate-induced yield changes. Existing land use models involving complex human decision making were limited to low spatial resolution and small domain [*Agarwal et al*., 2002]. Of the past studies that integrated climate-induced crop yield changes with socioeconomic drivers in land use projection, most were limited to national/subnational levels and thus could not provide the large-scale gridded land use information needed by climate models [*Schmitz et al*., 2014]. In addition, most previous models were limited to aggregated land use for all crops and could not provide information on individual crops needed for land and food policy-making and for the development of climate adaptation strategies. The algorithm of cropland projection (LandPro_Crop) of *Ahmed et al*. [2016] has recently been developed to address the need for land use information at individual crop level and for spatially distributed land cover data.

The LandPro_Crop algorithm is spatially explicit. In the present study, for application to West Africa, a resolution of 0.5° is used to match the resolution of crop yield simulated by DSSAT. The algorithm is based on an equilibrium between future demand and supply of food at the country level, and treats each country separately. Cropland expansion in each country is driven by the "supply deficit" for each and every crop, which is the difference between effective future demand of a particular crop and its supply from the present-day harvest areas at future yield of the crop. The algorithm then allocates available land to different crops to address the "supply deficit" following several simple rules that govern the conversion from naturally vegetated land to cropland, and multiple scenarios of decision making are considered. For example, the best scenario with science-informed decision making assumes:

1. Forest is preferred over grassland in making new land for crops, and grassland will be converted to cropland only if forest area within a country is depleted.
2. For multiple grid cells with the same type of natural vegetation within a particular country, the order of land conversion follows the descending order of future crop yield across grid cells.
3. The conversion and allocation of naturally vegetated land to different crops in a particular country follow the descending order of "supply deficit" in that country.

In addition to the above "best scenario," several alternative scenarios have also been developed to test the sensitivity of the model results by altering one or multiple rules listed above. For example, a "worst scenario" involves reversing the order mentioned in rules (2) and (3), and several intermediate scenarios represent different degrees of randomness in the decision making related to each of the rules.

The DSSAT-simulated future crop yield ($Y^{fu}_{DSSAT,ijk}$ for crop j at pixel k in country i) is not directly used by LandPro_Crop as input. Instead, it is first scaled by three factors (that are estimated based on parameters in present-day climate and are assumed to stay stationary in the future), as illustrated in equation (1). The first factor is the ratio of the observational crop yield ($Y_{SPAM,ijk}$) to the DSSAT-simulated present-day crop yield

($Y_{DSSAT,ijk}$), to correct the remaining DSSAT bias after calibration; the second is the ratio of the present-day harvesting area for the five major crops combined ($A_{M,ik}$) to the harvesting area of all crops combined ($A_{H,ik}$), to indirectly account for the impact of other crops ("minor crops") on future cropland distribution; the third is the ratio of present-day total harvest area ($A_{H,ik}$) to the present-day total area of physical land for crops ($A_{P,ik}$), to indirectly account for the impact of mixed crops farming. These are all captured in the following equation:

$$Y^{fu}_{i,j,k} = Y^{fu}_{DSSAT,ijk} \cdot \frac{Y_{SPAM,ijk}}{Y_{DSSAT,ijk}} \cdot \frac{A_{M,ik}}{A_{H,ik}} \cdot \frac{A_{H,ik}}{A_{P,ik}} \quad (1)$$

where $Y^{fu}_{i,j,k}$ is the future adjusted yield for crop j at pixel k in country i, to be used as input to LandPro_Crop. The present-day observed yield and harvesting area of each crop and the total physical area of all cropland within each grid cell were derived from the Spatial Production Allocation Model (SPAM) data [*You and Wood*, 2006; *You et al*., 2014] that were produced using a cross-entropy approach taking into account national and subnational production statistics, irrigation and rain-fed systems, prices, land use data, satellite imagery, biophysical crop "suitability" assessments, population density, and distance to urban centers.

3. Methodology and Experimental Design

3.1. The Asynchronous Coupling Approach

The four different models described above are asynchronously coupled to form a linked modeling framework. Specifically, for a given time slice, the RCM climate model and the economic model IMPACT will be run first, driven with output from GCMs; land cover map in the first RCM run will be specified according to present-day condition. The RCM climate output will be corrected for biases first (as detailed in section 3.4) before being used as the meteorological forcing to drive the crop model DSSAT. The DSSAT-simulated crop yields after adjustment (using equation (1)) and the effective food demands estimated by IMPACT will then be used as inputs to the cropland projection model LandPro_Crop. The LandPro_Crop-projected cropland expansion and the resulting loss of naturally vegetated land will then be used to update the land cover data in a new RCM simulation, and this alternation among the four models will continue.

A specific application of the asynchronous coupled modeling framework can take either an equilibrium approach or a transient approach. In the equilibrium approach, all simulations will be done for the targeted future time slice only, and the alternation among the four models should continue until all results converge. In practice, multiple iterations are necessary only if the land cover changes from LandPro_Crop are found to cause major changes in the projected future climates that are large enough to significantly alter the projected future crop yield changes. In the transient approach, each iteration represents a new time slice, and the iteration time step (i.e., the interval between adjacent time slides) technically can be one year or several years. In practice, however, the iteration time step should be long enough for crop land use activities to respond or adapt to the climate-induced yield changes. For this reason, the transient approach is subject to uncertainties related to the time scale of human adaptation. This paper focuses on interactive cropland-climate projections using the equilibrium approach; a companion paper will compare the two different approaches [*Ahmed et al*., 2017].

The rationale of using the asynchronous coupling approach is two-folded. First, it is by necessity due to the lack of a synchronously coupled model that encompasses all the important components and processes represented at the desired level of sophistication. Developing a synchronously coupled model that strikes a balance among the complexities of various submodels is a major undertaking, and is a long-term goal that motivated the study documented here. Experience and understanding developed from this asynchronous coupling study will help guide the design and development of a synchronously coupled model. Second, synchronously coupled models often suffer from "climate drift" (which occurs as a result of positive feedback among submodels enhancing biases in all models involved, e.g., *Wang et al*. [2015] and *Erfanian et al*. [2016]), while the asynchronous coupling approach can prevent or limit "climate drift" through correcting biases in the output of a submodel before passing it down to the next submodel. The asynchronous coupling approach therefore offers a desirable advantage in this aspect.

Conceptually, an important caveat associated with the use of asynchronous coupling is the potential inconsistency among the different models. For example, DSSAT includes simple treatment of water budget

calculations including evapotranspiration; however, in the RCM, all fluxes from the land surface that influence regional climate, including those from both naturally vegetated land and cropland, are calculated by the land surface model in the RCM. Similarly, the IMPACT model accounts for a much larger number of socioeconomic factors than the LandPro_Crop model, and some of those that are not accounted for in LandPro_Crop actually have implications for land use allocation. In practice, the impact of these inconsistencies on the model-projected future changes is likely to be small, but cannot be excluded without further improvement of the modeling framework that tightens the coupling among these models (which is a topic of follow-up research).

3.2. Experimental Design

In applying the regional modeling framework to West Africa, the RCM simulations are performed on a domain that spans approximately 20°S–35°N and 32°W–53°E at a 50 km horizontal resolution, with 18 vertical levels from surface to 50 hPa. ICBCs for the RCM include zonal and meridional winds, atmospheric temperature and humidity at all 18 levels, and surface air pressure and sea surface temperature, and are derived from global models participating in the fifth phase of the Coupled Model Intercomparison Project (CMIP5) [*Taylor et al*., 2012] models, and two different models are chosen, the MIROC-ESM [*Watanabe et al*., 2011] and the CCSM4 version of CESM [*Neale et al*., 2012; *Meehl et al*., 2013]. Corresponding to each of the two global models, a pair of simulations are conducted in this study: a "Present" simulation for the period 1981–2000, for which the ICBCs are derived from the global model historical simulations; a midcentury "Future" experiment for the period 2041–2050, for which the ICBCs are derived from the global model RCP8.5 experiment. The GHGs concentrations are based on historical observations for the "Present" simulation and RCP8.5 pathway for the "Future" experiment. Note that before midcentury, differences among various RCPs are small relative to inter-model variations. In the main "Future" experiment, the cropland allocation follows the "best scenario" with science-informed decision making; several sensitivity experiments featuring alternative scenarios of cropland allocation examine the impact of each of the rules for land allocation, by reversing some or all of the orders stated in section 2.4 or randomizing the priority rank.

In addition to the "Future" projections that make use of the complete system shown in Figure 1, two additional types of projections are designed to attribute the projected future changes. One type of attribution experiments (Future_SE) focuses on separating the impact of socioeconomic factors from that of climate change on cropland expansion. It makes use of the present-day crop yield in LandPro_Crop to project future cropland expansion therefore neglects the role of climate-induced yield change as the biophysical driver for land use. The resulting cropland expansion is therefore caused solely by socioeconomic factors. Differences in cropland expansion between the "Future" and "Future_SE" experiments reflect the impact of climate change. Another type of attribution experiments (Future_noLUC) focuses on separating the impact of projected land use land cover changes from that of the GHGs on regional climate. Specifically, land use land cover in a RCM future run is prescribed according to present-day conditions in Future_noLUC. Therefore, the projected climate changes (i.e., differences between Present and Future_noLUC) are caused solely by the increase of GHGs concentrations, while the differences between "Future" and "Future_noLUC" reflect the impact of land use land cover changes on regional climate.

In projecting future climate changes and cropland expansion using the regional modeling framework shown in Figure 1, output from GCMs are used not only as ICBCs for the RCM submodel but also as global forcing for the IMPACT submodel. As alluded to in section 2.3, the consideration for GCM-related uncertainties in IMPACT takes a different approach from GCM-related uncertainties in RCM. Four IMPACT runs were conducted, each driven with output from a different global model (GFDL-ESM2M, HadGEM2-ES, IPSL-CM5A-LR, and MIROC-ESM, respectively); instead of retaining four different projections of future food demands for each country, the ensemble average of the four IMPACT runs was used to estimate the demands for food (that are used as inputs to the LandPro_Crop model). This approach is preferred because differences in food demands from the four IMPACT runs are very small for both the total demand and effective demand (Figure 3). As global climate influences regional food production through its impact on international trade therefore on food price, the ensemble average of the four runs is expected to reduce the uncertainties in the effective food demand caused by uncertainties of global climate projections. To examine the impact of international trade on cropland expansion, a sensitivity test is also conducted using the total demand (as opposed to the effective demand) as input to LandPro_Crop to estimate cropland expansion for the hypothetical scenario of zero international trade.

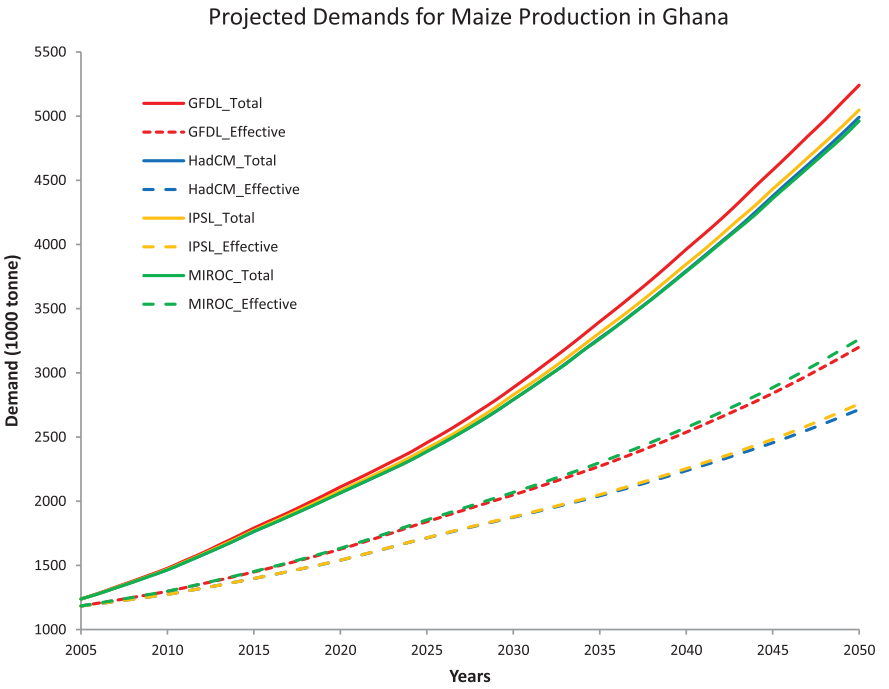

Figure 3. Total demand and effective demand for maize projected by IMPACT driven with global climates from four different models, using Ghana as an example.

Table 1 list all the experiments described above. Note that some of the experiments make use of the comprehensive modeling system shown in Figure 1, while others use a subset of the models depending on the nature and focus of each specific experiment.

3.3. Initial Conditions for Land Use and Land Cover

The present-day harvest area for each of the five major crops and total physical cropland area (as a fraction of each 0.5° grid cell, Figure 4) derived from the SPAM 2005 data (available at www.mapSPAM.info) are used as LandPro_Crop input to derive area-related parameter values in equation (1) and to provide cropland initial conditions at the individual crop level. Millet, sorghum, and peanut are more prevalent in the Sahel region, and maize and cassava are more prevalent in the southern part of West Africa. Present-day cropland coverage shows a strong east-west contrast, exceeding 90% in some areas over Nigeria but below 10% in most of the region west of 5°W.

Other initial conditions for LandPro_Crop include the present-day fractional coverage of forest area and grassland in each grid cell, which are derived by summing up the coverages of corresponding PFTs from the global data set of *Lawrence and Chase* [2007]. Although the *Lawrence and Chase* [2007] data do not provide information on cropland coverage at the individual crop level, it does include the grid-level total cropland coverage, which was derived from the data set of *Ramankutty and Foley* [1999] and differs slightly

Table 1. Summary of Experimental Design

Experiments Type	Focus of Analysis	Time	ICBCs for RCM	Land Cover	LandPro Scenario (s)	Crop Yield	Food Demand
Present	Climate	1981–2000	ERA-In, MIROC, CESM	Present prescribed	n/a	n/a	n/a
Future	Climate and cropland	2041–2050	MIROC, CESM	Future projected	Best scenario	Future	Effective demand
Future_alts (multiple)	Cropland	2041–2050	MIROC, CESM	Future projected	Alternative scenarios	Future	Effective demand
Future_noTrade	Cropland	2041–2050	MIROC, CESM	Future projected	Best scenario	Future	Total demand
Future_SE	Cropland	2041–2050	MIROC, CESM	Future projected	Best scenario	Present	Effective demand
Future_noLUC	Climate	2041–2050	MIROC, CESM	Present prescribed	Best scenario	Future	Effective demand

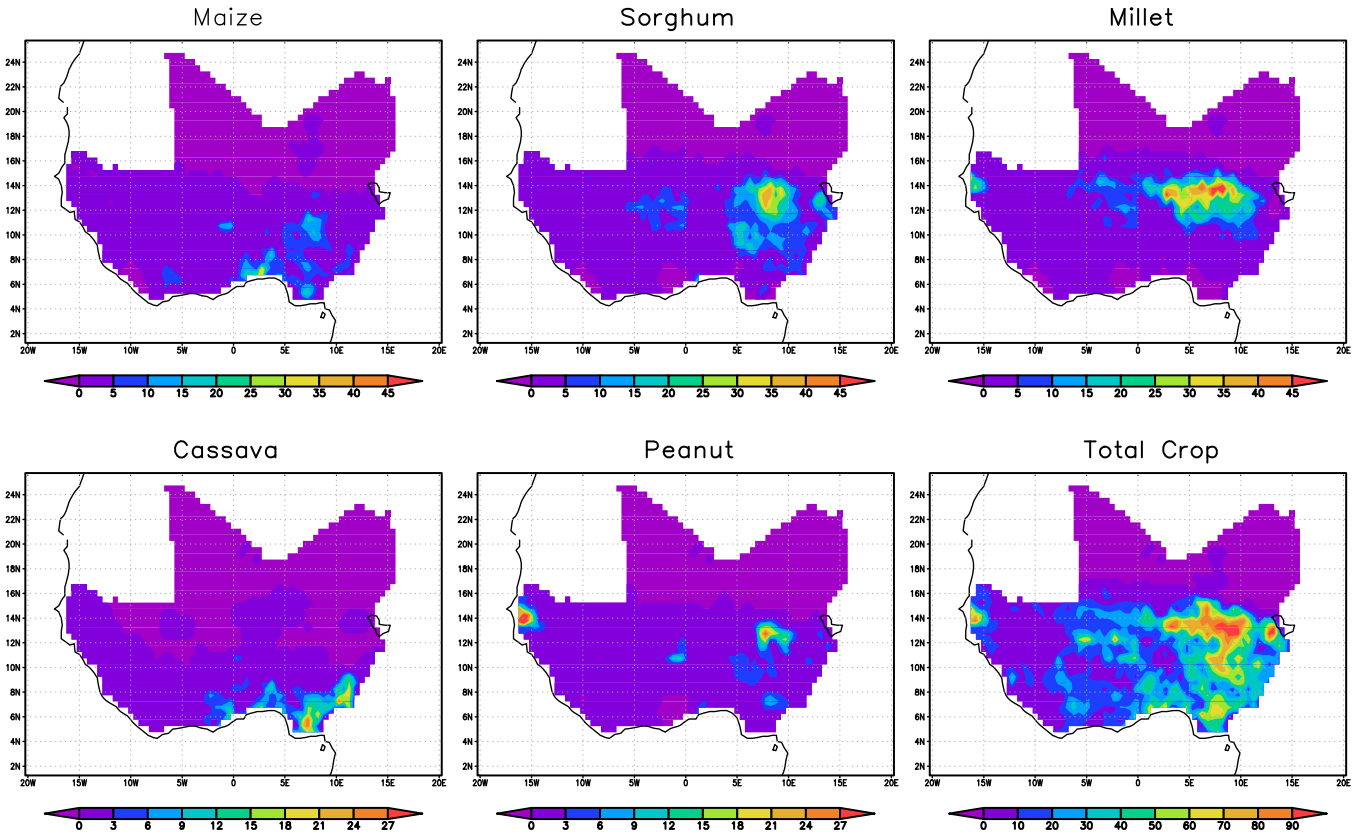

Figure 4. Present-day distribution of harvest areas (as a percentage of the total grid cell area) for all five major crops (as the initial conditions for LandPro_Crop), and the total cropland fractional coverage (as the initial land cover specification for RegCM-CLM), based on SPAM data. Note that the sum of harvest areas can exceed the physical areas corresponding to the total cropland fractional coverage due to the existence of mixed crops farming.

from the SPAM data. For consistency, the fractional coverage of forest and grassland from *Lawrence and Chase* [2007] were adjusted proportionally to accommodate a combined cropland coverage equivalent to that from SPAM (Figure 4, bottom right). This was necessary because, in both LandPro_Crop and RegCM4.3.4-CLM4.5, the fractional coverage of all plant functional types (which in West Africa include crops, C4 grass, tropical broadleaf evergreen trees, tropical broadleaf drought deciduous trees, shrubs, and bare soil) should sum up to 100% within each grid cell.

3.4. Regional Climate Bias Correction

To simulate the present-day crop yield, we drive DSSAT with the 0.5° resolution daily climate data from the Princeton University gridded meteorological forcing data set [*Sheffield et al*., 2006]; to project future crop yield using DSSAT, we rely on future climate forcing derived from the RCM. As evident from Figure 1, the RCM climate driven with ICBCs from both MIROC-ESM and CESM shows systematic biases in West Africa, which necessarily will influence the RCM-produced future climate. A quantile mapping approach [*Ahmed et al*., 2013] is used to correct the model biases in future climate projections, assuming that the statistical relationship between the probability distributions of model climate and actual climate in the present-day will remain unchanged in the future [*Wilby*, 1998; *Boé et al*., 2006]. This follows a three-step procedure:

Step 1 (Detrending): the RCM output for both the present and future climate were first resampled to a 0.5° grid system to match the resolution of the Princeton University data that is used as the observational reference for present-day climate, and the resampled future climate will be detrended based on a linear regression of the model climate with time, over the period covering both the past and future climate. The linear regression relationship used for detrending the data will be saved for use in Step 3.

Step 2 (Quantile Mapping): a quantile mapping between the Cumulative Distribution Function (CDF) for the observational data and the CDF for the RCM resent-day climate during the same time period will be developed first. For each value of a detrended future climate variable, the corresponding exceeding probability will then be found from the RCM CDF, and the threshold value at the same exceeding probability from the observed climate CDF will be taken as the bias-corrected output.

Step 3 (Adding Trend Back): the trend taken off the RCM future climate in Step 1 will be added back to output from Step 2 to obtain the bias-corrected future climate variable value.

This quantile mapping approach corrects model biases in both the mean climate and probability distribution; the separation of the model future trend from the quantile mapping prevents the otherwise extensive need for extrapolation (that could disproportionally influence future climate extremes) during the quantile mapping procedure.

4. Results

4.1. Future Scenarios of Agricultural Changes and Attribution

The projected future yield changes of major crops are dominated by a decreasing trend, with the exception of sorghum (Figure 5). Among the environmental variables that are important for crop growth, both CO_2 concentration and temperature will increase substantially, and the magnitude and spatial pattern of warming are similar between the projections driven by the two GCMs (results not shown). The CO_2 "fertilization" effects on future crop yield were found to be negligible [*Ahmed et al*., 2015], a result consistent with findings from previous studies [e.g., *Berg et al*., 2013]. This is primarily because the concentration in the "Present" simulation is already very close to the level of photosynthesis saturation (400 ppmv) for C4 crops. The general decrease of yield is a result of the strong GHG-induced warming and associated heat stress as well as the resulting increase of total evapotranspiration leading to drought.

Beyond the dominant signal of a reduced yield, both the spatial pattern and magnitude of the relative yield changes differ substantially between the two projections driven with MIROC-ESM and CESM, and differ substantially among different crops under the same climate (Figure 5). These differences reflect not only the complexity and genetic variation of crop responses to environmental factors but also the confounding effects of the highly heterogeneous precipitation changes and related solar radiation changes (Figure 6). For precipitation and solar radiation, both the direction and magnitude of projected changes differ significantly between the two projections, and show strong spatial contrast during the primary growing season in June, July, August, and September (Figure 6). While an increase of precipitation improves water availability therefore favors crop growth, the cloudiness (therefore reduced sun light) associated with too much precipitation could potentially reduce crop yield. Also, the same amount of precipitation change at different stages of crop development may have very different yield outcome. For example, sorghum yield is projected to increase significantly over most of the domain under the CESM-driven future climate, but is projected to increase moderately over a small fraction of the domain and decrease elsewhere under the MIROC-ESM-driven climate (Figure 5). Precipitation change in the CESM-driven projection (Figure 6, right) includes primarily a dry signal in June-July-August and a wet signal in September reflecting a delayed monsoon demise, with slight changes in surface insolation. This increased water availability during the grain filling stage of sorghum in September is a major factor contributing to the projected increase of yield; maize and millet due to their shorter growing season reach maturity by September therefore cannot take full advantage of the increased late-season precipitation. In the MIROC-ESM-driven projection, a rather dramatic increase of precipitation especially in the eastern part of the domain is accompanied by a dramatic decrease of surface solar insolation throughout the growing season (Figure 6). These two have compensating effects on crop yield, leading to a high degree of spatial heterogeneity in the response of maize and sorghum yields (Figure 5, left).

In addition to the spatially distributed yield changes, country-level yield statistics for the five major crops were also analyzed focusing on the long-term mean and range of inter-annual variation of the country average yield (results not shown). Despite the differences in spatial pattern of crop yield changes, for maize, millet, cassava, and peanut in all countries, the two projections of future yield changes are qualitatively similar, both featuring a decrease of the mean yield; for sorghum, consistent with the distributed changes (Figure 5), the projected future changes are mixed, with a slight decrease of the mean in some countries and increase in others. Moreover, in most countries and for all five crops, regardless of whether CESM or MIROC-ESM is

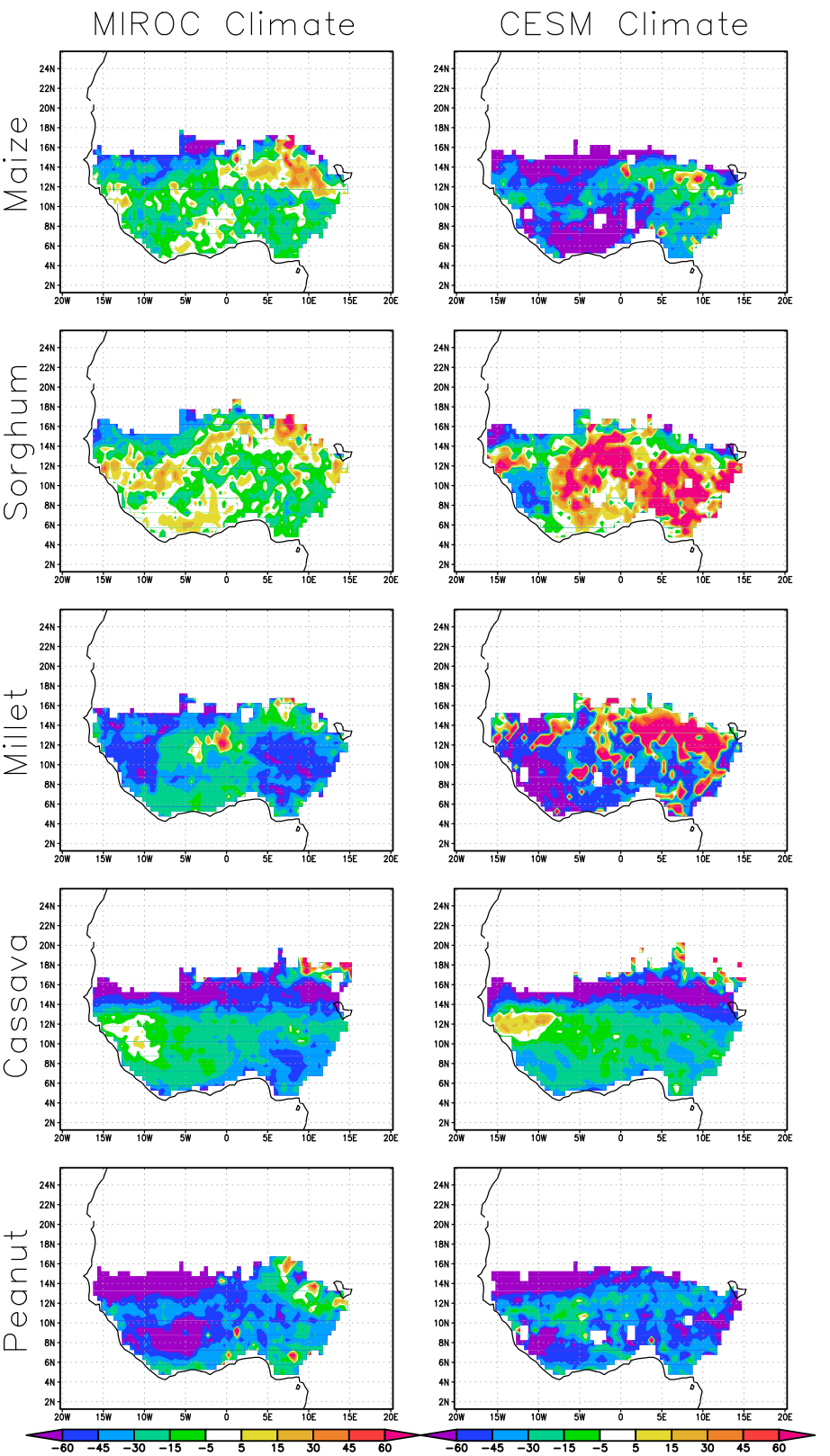

Figure 5. Future changes of crop yield for maize, sorghum, millet, cassava, and peanut, as projected by the regional system driven with the (left) MIROC-ESM and (right) CESM (in %).

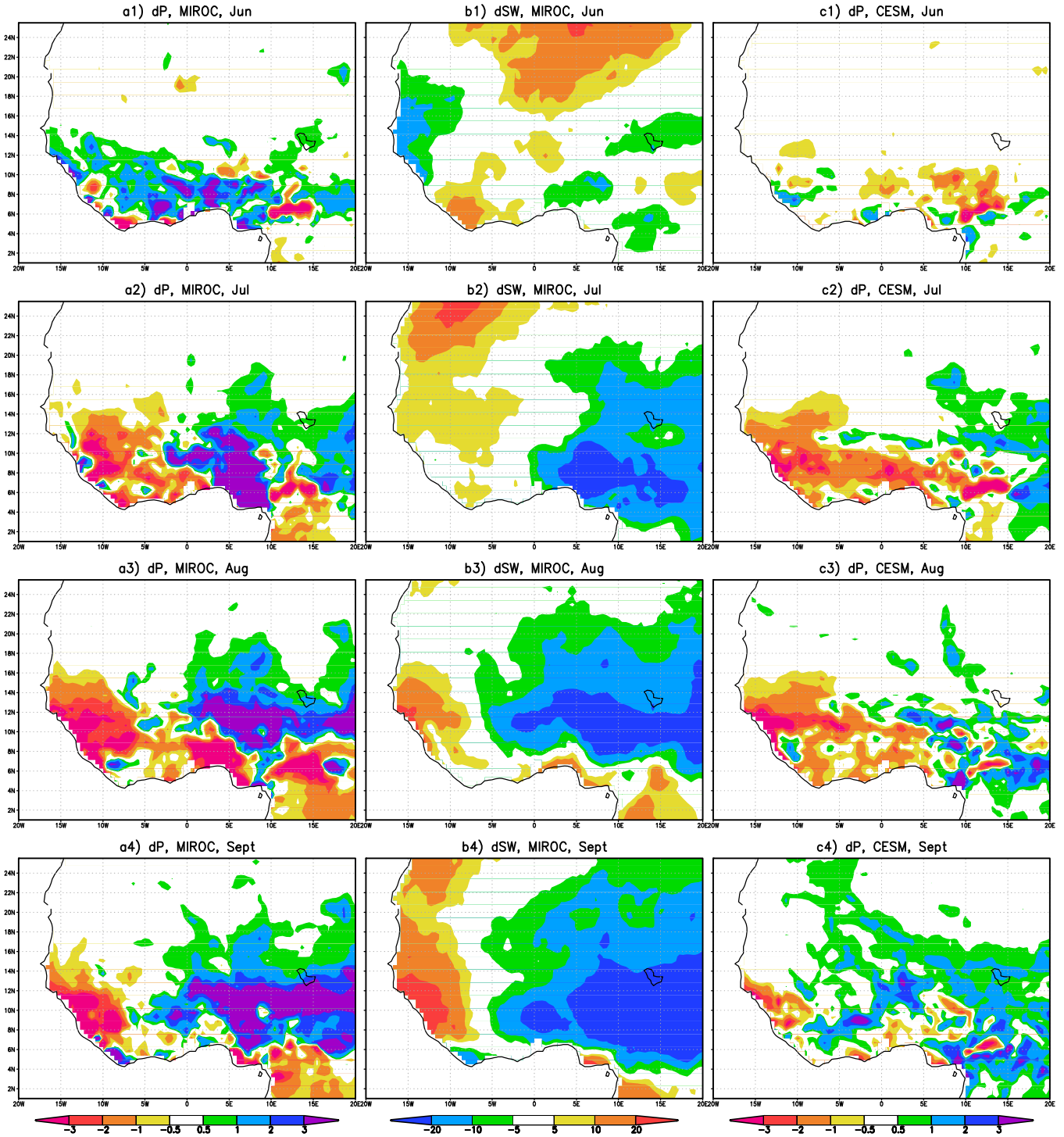

Figure 6. (a1–a4 and b1–b4) Projected changes in precipitation (mm/d) and in surface solar radiation (W/m^2) when driven by ICBCs from MIROC-ESM and (c1–c4) projected precipitation changes driven by ICBCs from CESM during each month of the common growing season June, July, August, and September.

used to drive the regional climate model, a significant increase in the range of inter-annual variation of crop yield is projected, which suggests a more volatile future food supply system [*Ahmed et al.*, 2015].

The projected decrease of crop yield and increase of demand together serve as drivers for future agricultural expansion. The total cropland expansion is remarkably similar between the CESM-driven and MIROC-driven projections (Figure 7). The fastest growth would be in the eastern half of West Africa, followed by the region

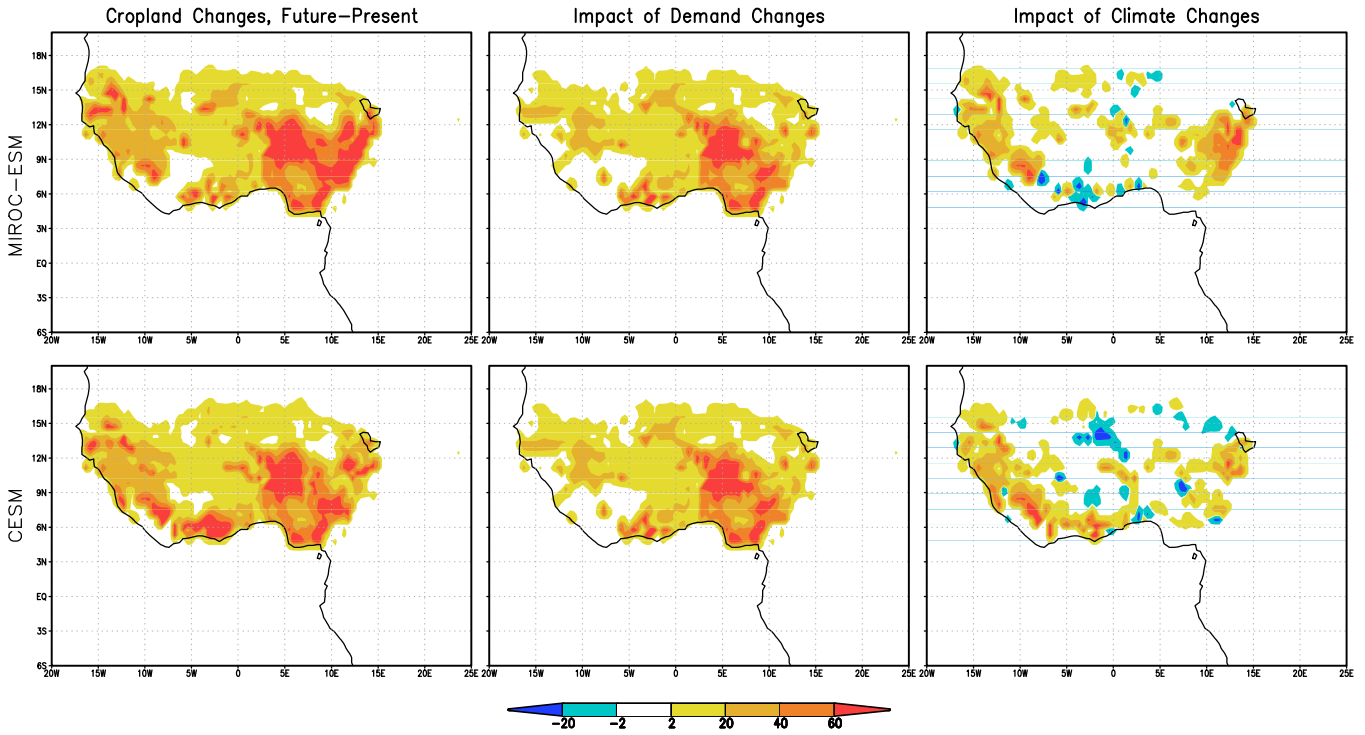

Figure 7. (left) Projected future changes of cropland area (in % of the grid cell area) by midcentury ("Future-Present") when the Regional Climate Model is driven by ICBCs from (top) MIROC-ESM and (bottom) CESM, and (middle) the cropland changes attributable to food demand changes ("Future_SE-Present") and (right) those attributable to climate-induced crop yield changes ("Future-Future_SE").

near the southwest coast. However, the two hotspots are attributable to different causes. The one in the eastern half is primarily caused by increased food demand, while the one along the southwest coast is primarily due to climate change (through reducing crop yield). Over most of the domain, however, future increase of cropland coverage is associated with food demand; the spatial pattern of the demand-induced expansion shows an east-west contrast that resembles the present-day cropland distribution (except for areas where the already high cropland coverage leaves little room for further expansion), which suggests a stronger socioeconomic disparity in the future. The impact of climate change on agricultural expansion is significant primarily over the western half of West Africa especially in the southwest coastal region.

The projected cropland expansion is at the expense of naturally vegetated land (Figure 8). The partition between deforestation and desertification however is dictated by the assumption in LandPro_Crop that conversion of grassland to cropland does not start until woodland is depleted. The presence of grassland loss in Figure 8 therefore indicates complete deforestation in a country. The assumption of preferential conversion of woodland to cropland was made to reflect historical trend [e.g., *Burney et al.*, 2010; *Hurtt et al.*, 2011] that may have resulted from the need to preserve grassland for pasture/animal grazing and the generally more fertile soil in newly deforested land. Reversing the order between forest and grassland would lead to significantly different results on changes of the natural vegetation cover; the impact on cropland expansion would be also significant especially in the western part of West Africa and along the coast where present-day forest coverage is high. Similar to the cropland expansion, the distribution of natural vegetation cover loss shows negligible difference between the projections driven with the two GCMs.

Among the many uncertainty factors considered in the sensitivity tests described in section 3, the projected cropland expansion is most sensitive to two: the level of international trading and the sequence of land conversion among multiple grid cells in which land is available. An extreme example of each is given in Figure 9 based on CESM-driven projections. Without changing any rules and assumptions in the LandPro_Crop model, if international trading were not allowed (i.e., only domestic production can be used to meet domestic demand), the projected cropland expansion would be much faster (Figure 9a, relative to Figure 7). With

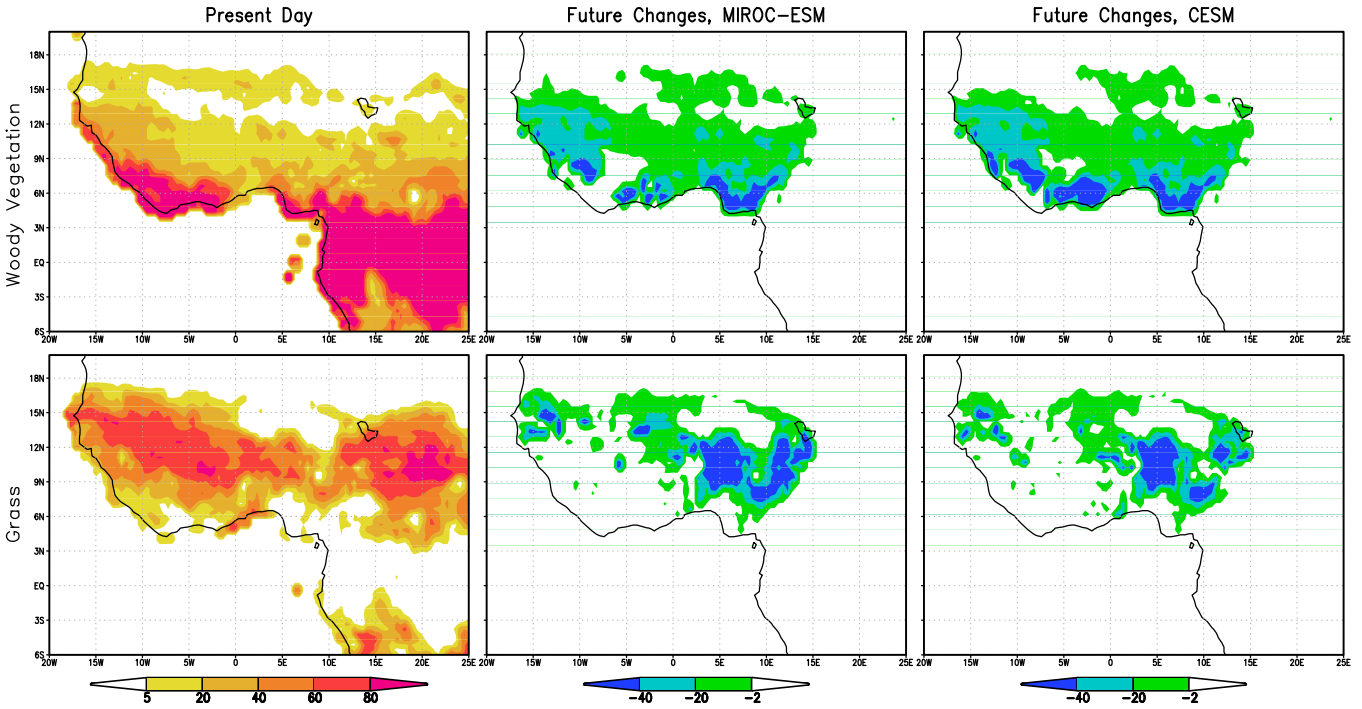

Figure 8. (top) Woody vegetation and (bottom) grass coverage (in % of the corresponding grid cell area): (left) present-day distribution, projected future changes when RegCM is driven by LBCs from (middle) MIROC-ESM and (right) CESM.

the projected international trade but reversing the order of land conversion to create an extreme scenario (in which the least productive land was used up first before more productive land was considered for conversion to cropland), the cropland expansion would be dramatically faster (Figure 9b, relative to Figure7). The order of land allocation among different crops has a negligible impact on the overall cropland expansion. Given past and present-day practices, the extreme scenarios of cropland expansion in Figure 9 are highly unlikely. Our study on the potential impact of land use feedback to regional climate (section 4.2) is therefore based on the "best scenario" land cover changes shown in Figures 7 and 8.

4.2. Future Scenarios of Climate Changes and Attribution

Future precipitation changes during the peak monsoon season projected by RegCM-CLM driven with both MIROC-ESM and CESM feature a west-east dry-wet contrast (Figure 10, middle). This general pattern of future precipitation changes was also found in the multiGCM ensembles [*IPCC*, 2013] as well as in the ensemble of regional climate projections driven by multiple GCMs [*Saini et al*., 2015; *Erfanian et al*., 2016]. However, the two projections in Figure 10 also demonstrate clear differences: in the projection driven with MIROC-ESM, the dry signal is found in the western half of West Africa and also over central Africa, and the wet signal is much stronger and extends from West Africa to the Middle East; in the projection driven with CESM, the dry signal extends over most of West Africa, and a relatively weak wet signal covers central Africa and the eastern half of Sahel.

Majority of these projected changes, including the east-west contrast, are caused by GHG concentration changes. Land cover changes related to the projected cropland expansion would enhance the east-west contrast of future precipitation changes in the model (Figure 10). Moreover, despite the significant differences in future precipitation change projected by the two different models, the contribution from land cover changes shows a high degree of similarity between the two, with a drought signal in the west and a dominantly wet signal in the east. In some areas of the western West Africa, the magnitude of precipitation changes caused by land use changes even rivals that of the CO_2-induced changes (Figure 10, right column versus left column), and this statement holds for projections driven with LBCs from both GCMs. Not surprisingly, since projected land cover changes were only applied to West Africa, the effects on precipitation elsewhere are weak.

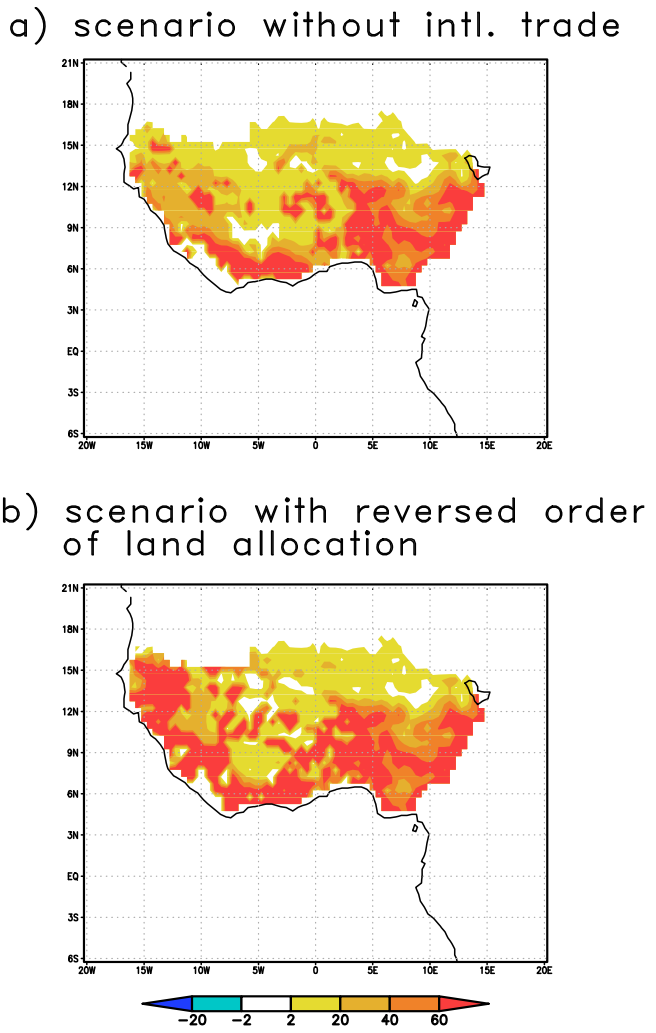

Figure 9. Projected future changes of cropland fractional coverage (as a percentage of the corresponding grid cell area): (a) for a hypothetical scenario of no international trade, and (b) for a land use scenario that includes international trade but reverses the order of land conversion in LandPro_Crop (i.e., using up the least productive land first).

The rather robust spatial pattern of LUC-induced precipitation changes, with a decrease in the west and an increase in the east (and its surrounding areas), appears to deviate from the general notion of land cover degradation causing precipitation to decrease. Part of this deviation has to do with the location, spatial extent and heterogeneity of the projected land cover changes in this study, and part has to do with the nonlocal impact of land cover changes. Figure 11 presents the LUC-induced differences during the monsoon season (June-July-August) for several variables related to the surface energy and water budgets, using the projections driven by the MIROC-ESM as an example. Results based on projections driven by the CESM model (not shown) are qualitatively similar. The decrease of LAI resulting from land cover changes during the JJA season is highly heterogeneous, and for the most part is rather small (less than 0.4, Figure 11a1). Loss of vegetation cover tends to reduce evapotranspiration (ET) therefore local supply of moisture over most of the domain (Figure 11b1), which contributes to the decrease of precipitation.

The loss of woody vegetation cover reduces the surface roughness therefore increases the speed of surface winds that are southwesterly (Figure 11a3). This accelerated transport of moisture toward the northeast contributes to a decrease of atmospheric moisture flux convergence in the south and west and an increase downwind in the north and east (Figure 11b2). Precipitation changes (Figure 10) are dominated by the decrease of local moisture supply through ET in the western Sahel region, and by changes in moisture flux convergence elsewhere.

The LUC-induced albedo increase shows strong heterogeneity too, and is less than 0.01 in most of the domain (Figure 11a2). As a result, surface net radiation slightly decreases over most of the domain (except over the Guinea Coast where net radiation increases). The spatial pattern of LUC-induced ET changes resembles that of the net radiation changes for most of the domain where ET is energy limited (Figures 11b1 and 11c2). Despite the decrease of net radiation, a warm signal is found over West Africa due primarily to the decrease of evaporative cooling (Figure 11c3). Moisture storage in the top 10 cm of the soil is projected to decrease in most of West Africa and increase elsewhere (Figure 11b3).

Among all subregions of West Africa, the Guinea Coast is the wettest where hydrological processes are subject to energy limitations. As a result, climate response to land cover changes is strongly influenced by cloud effects. For example, despite a decrease of LAI, ET from the Guinea Coast increases due to an increase of net radiation; despite an increase of surface albedo, surface net radiation increases as a result of higher solar insolation due to reduced precipitation therefore reduced cloudiness. This underlies the contrast between the Guinea Coast and elsewhere in the response of climate variables to land cover changes.

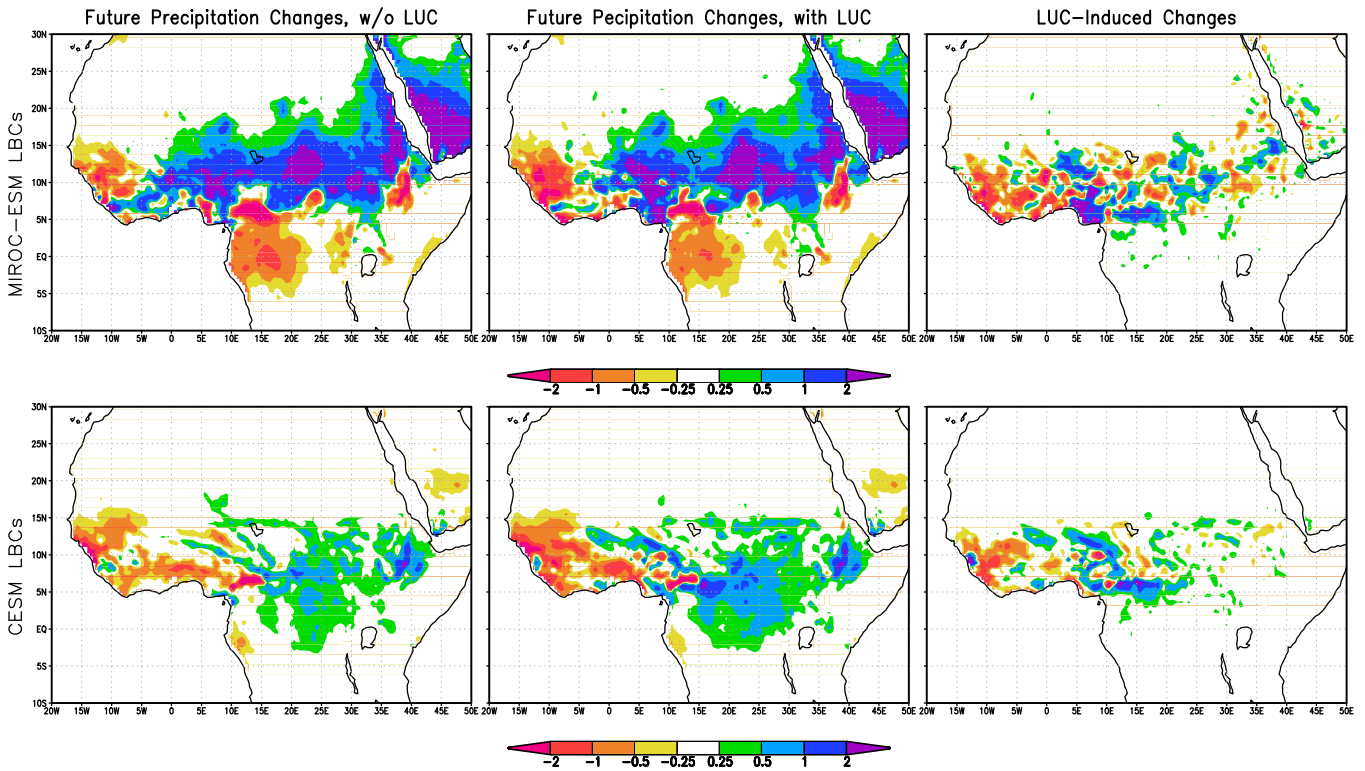

Figure 10. Projected future changes of JJA precipitation (in mm/d) by midcentury driven with LBCs from (top) MIROC-ESM and (bottom) CESM, respectively, (left) with present-day land use ("Future_noLUC-Present"), (middle) with projected "best scenario" of future land use changes ("Future-Present"), and (right) the LUC-induced differences (as "Future-Future_noLUC").

5. Conclusions and Discussion

Agricultural land use alters regional climate by modifying surface water, energy, and momentum fluxes; changes in climate influence land use activities through their impact on crop yields and cropping patterns. This study tackles the critical linkages within the coupled natural and human systems in West Africa focusing on the interactions between agricultural land use and the changing regional climate. Using an asynchronously coupled modeling framework involving four different models, we assess the role of land use as a climate change forcing (relative to the GHGs concentration changes) and the role of climate change as the biophysical driver (relative to the socioeconomic drivers) for agricultural land use changes. The main findings are:

1. Socioeconomic developments would be the dominant driver for future cropland expansion in the eastern part of West Africa, where current cropland coverage is already high; climate changes would be the primary driver for future cropland expansion in the western part.
2. The projected agricultural expansion would cause a strong dry signal in the western part of West Africa and a wet signal in the eastern part downwind. Over a substantial portion of West Africa, the strength of the LUC-induced signals of precipitation changes is comparable to that of the GHG-induced precipitation changes, and the east-west contrast of LUC-induced precipitation changes is closely related to the regional monsoon circulation pattern and its response to land cover changes.

Based on results from this study, it is apparent that land use-climate interactions would enhance the CO_2-induced precipitation changes, especially the projected contrast between changes in the east and west portions of West Africa. The LUC-induced increase of precipitation downwind in the northeast portion of the focus region is qualitatively similar to the modeled precipitation response to deforestation in Nigeria and elsewhere in West Africa [*Abiodun et al.*, 2012]. This response is likely a result of the specific regional monsoon circulation pattern and therefore may not be generalized for other regions. Different than most previous studies that impose idealized (and often spatially uniform) land cover or land cover changes in climate models, land cover changes in this study are projected by a coherent modeling system based on realistic

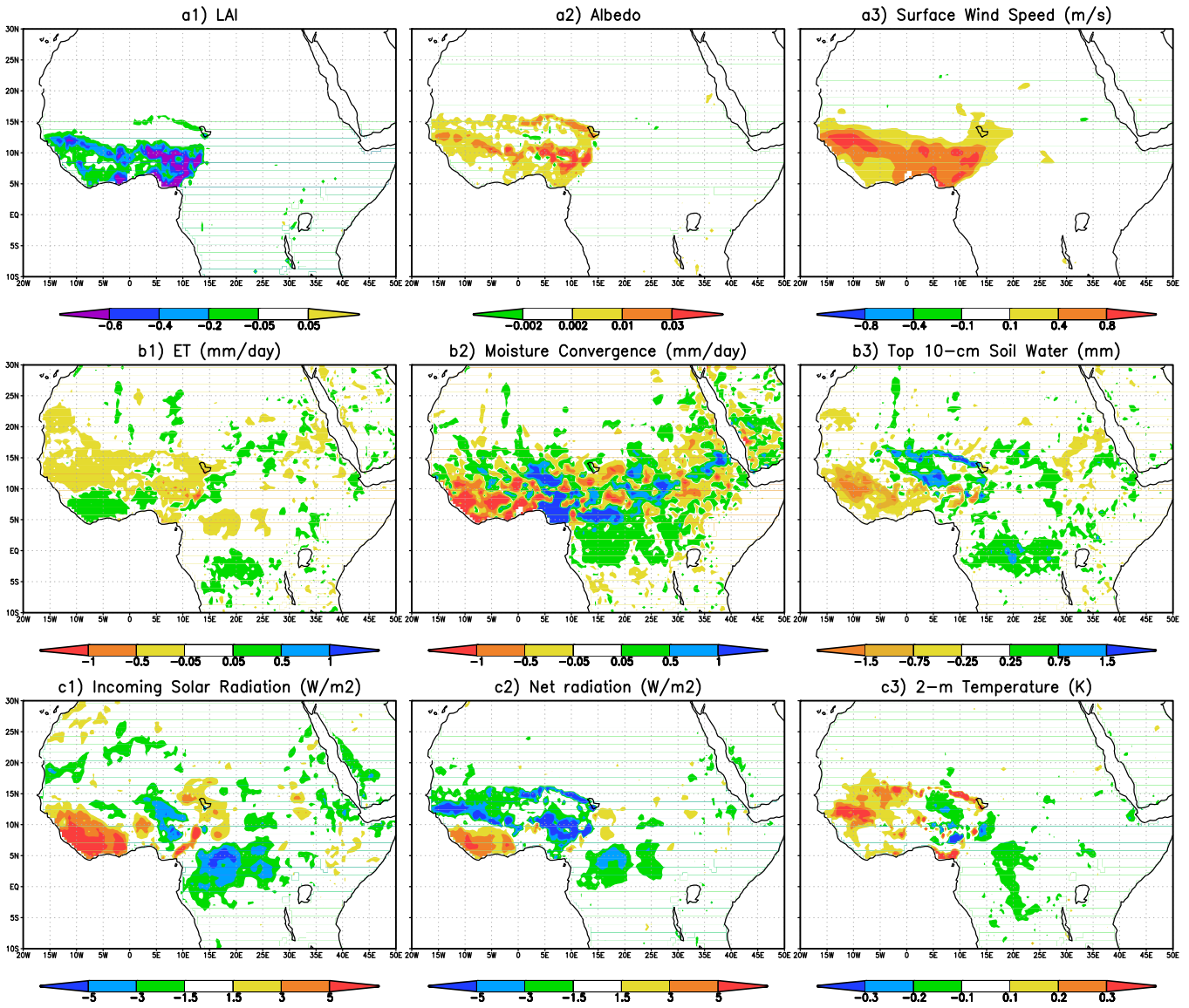

Figure 11. TheUC-induced differences in LAI, albedo, surface wind speed, ET, moisture flux convergence, top 10 cm soil moisture (in equivalent water depth), surface insolation, surface net radiation, and surface air temperature, using projections driven with the MIROC-ESM LBCs as examples.

increase of food demand and climate changes and show a higher degree of spatial heterogeneity. While the response found in this study is more complex than the general notion of "land cover degradation causing less precipitation," the fundamental mechanisms of local climate response to land cover changes through surface property changes (in albedo, Bowen ratio, and roughness) [*Wang et al.*, 2015] remain largely the same. What is different here is that, given the magnitude, location, and spatial extent of land cover changes, the response of regional circulation to these changes is more dominant, leading to the seeming complexity of the climate response.

In addition to modifying land-atmosphere mass, momentum, and energy flux exchanges, land cover changes can also influence regional climate through their impact on atmospheric aerosol loading due to mineral dust and biomass burning emissions. For example, past studies suggested that in West Africa mineral dusts would cause precipitation to decrease [e.g., *Ji et al.*, 2016, 2017]. Both the location and the magnitude of aerosol sources depend heavily on vegetation cover and agricultural land use as well as their seasonality. However, in most climate models including the RCM used in this study, dust and biomass burning emissions are either not considered or treated separately from land use processes, which leads to an

incomplete account for the impact of cropland expansion in our study. Linking aerosol emissions with agricultural land use at the seasonal time scale (therefore accounting for the presence of land cover during the growing season and absence after harvest during the dry season) would be a necessary next step to address the aerosols-related uncertainties.

Qualitatively, the projected changes in future cropland expansion and regional climate as well as their attribution in the projections driven by ICBCs from the two GCMs are remarkably similar, due to the low sensitivity of the RCM climate change to the driving GCMs [*Saini et al*., 2015]. The sensitivity of the IMPACT-projected food demand to GCM climates is rather low too. Therefore, addressing uncertainties from climate models would need to involve a different RCM as opposed to more GCMs. The experimental design, using a regional modeling framework with prescribed past and RCP8.5 future CO_2 concentrations, precludes the consideration for the contribution of deforestation to atmospheric CO_2 concentration changes (therefore precludes the feedback to carbon dynamics).

Results and findings from this study are subject to uncertainties from three major sources related to human decision making on crop productions. One is the order in which naturally vegetated land is converted to agricultural land for different crops, with the "Best Scenario" following the three rules specified in section 2.4 representing a science-informed decision making. Results analysis and conclusions drawn above are based primarily on this conservative scenario. Sensitivity experiments in this study suggested that the spatial extent and magnitude of the projected cropland expansion could be significantly higher in a "worse scenario." Moreover, the assumption to deplete forestland before grassland has complex implications for climate feedback. On one hand, a more random sequence of converting naturally vegetated land to cropland would result in a faster cropland expansion, which could have a more significant impact on climate; on the other hand, it would also result in a larger degree of surface heterogeneity, which could reduce the climatic impact of land cover changes. The second source of uncertainty related to human decision making is the lack of consideration for agricultural intensification and some adaptation strategies that farmers customarily make in response to changing economic and environmental conditions [*Mendelsohn et al*., 1994]. The underlying hypothesis that agricultural expansion is favored over intensification is based on past and present practices in West Africa, and it may or may not hold in the future especially given the rising pressure from a rapidly warming climate. The potential increase of fertilizer application and labor input, expansion of irrigation, and switch to more heat- or drought-resistant cultivars (when feasible) would all reduce the impact of climate change on cropland expansion (and its feedback to climate). The third source of uncertainty is related to the size of international trade. For most countries in West Africa, import addresses a substantial fraction of food demand, while future trade (therefore the accuracy of its projection) can be heavily influenced by national economic policies and international food policies. To some extent, these uncertainties are of similar nature to those of future GHGs concentration pathways/scenarios, and may justify the creation of their own future scenarios. These uncertainties should be tackled in follow-up studies involving close collaboration with social and political sciences.

Climate-induced decrease of crop yield is an important driver for the projected cropland expansion in this study. The future crop yield in the model did not benefit much from the physiological effects of CO_2 concentration increase, due primarily to the fact that the present-day CO_2 concentration is already close to the saturation level for C_4 crops. However, nitrogen and phosphorus limitation is an important confounding factor, especially given the generally low level of fertilizer input in the region. Field experiments have shown that crop yield response to CO_2 concentration changes depends on nitrogen and water availability [e.g., *Long et al*., 2006; *Tubiello et al*., 2007]. The confounding effects of climate, CO_2, and nutrient on crop yield and how they may influence the future projections should be addressed in follow-up studies.

While West Africa is used here as a case study, the applicability of the modeling framework is not limited to West Africa. It can be translated to other developing regions in Africa and in other continents. For the modeling framework to be applicable to developed regions, the LandPro_Crop model will need to be modified to reflect the effect of specific land use policies in place and the effects of agricultural intensification that plays a more important role in developed countries. The findings on the relative importance of climate change and socioeconomic factors in driving land use change, and on the extent to which land use changes modify the GHG-induced climate changes, are likely to be region specific.

Acknowledgments
This study was supported by funding from NSF for a collaborative EaSM project (AGS-1049017, AGS-1048967, and AGS-1049186). Computational support was provided by NCAR Yellowstone (UCNN0001). We thank the two anonymous reviewers for their constructive comments toward an earlier version of this paper. All data are archived at the Hydroclimatology and Biosphere-Atmosphere Interactions group at the University of Connecticut and are available for download upon request (guiling.wang@uconn.edu).

References

Abiodun, B. J, J. S. Pal, E. A. Afiesimama, W. J. Gutowski, and A. Adedoyin (2008), Simulation of West African monsoon using RegCM3 Part II: Impacts of deforestation and desertification, *Theor. Appl. Climatol.*, *93*(3-4), 245–261.

Abiodun, B. J., Z. D. Adeyewa, P. G. Oguntunde, A. T. Salami, and V. O. Ajayi (2012), Modeling the impacts of reforestation on future climate in West Africa, *Theor. Appl. Climatol.*, *110*, 77–96, doi:10.1007/s00704-012-0614.

Agarwal, C., G. M. Green, J. M. Grove, T. P. Evans, and C. M. Schweik (2002), A review and assessment of land-use change models: Dynamics of space, time, and human choice, *Rep. GTR NE-297*, 61 pp., U.S. Dep. of Agric., For. Serv., Northeastern Res. Stn., Newton Square, Pa.

Ahmed, K. F., G. Wang, J. Silander, A. M. Wilson, J. M. Allen, R. Horton, and R. Anyah (2013), Statistical downscaling and bias correction of climate model outputs for climate change impact assessment in the U.S. northeast, *Global Planet Change*, *100*, 320–333.

Ahmed, K. F., G. Wang, M. Yu, L. Z. You, and J. W. Koo (2015), Potential impact of climate change on cereal crop yield in West Africa, *Clim. Change*, *133*, 321–334, doi:10.1007/s10584-015-1462-7.

Ahmed, K. F., G. Wang, L. Z. You, and M. Yu (2016), Potential impact of climate and socioeconomic changes on future agricultural land use in West Africa, *Earth Syst. Dyn.*, *7*, 151–165, doi:10.5194/esd-7-151-2016.

Ahmed, K. F., G. Wang, L. Z. You, R. Anyah, C. Zhang, and A. Burnicki (2017), Projecting regional climate and cropland changes using a linked biogeophysical-socioeconomic modeling framework: 2. Transient dynamics, *J. Adv. Model. Earth Syst.*, *9*, 377–388, doi:10.1002/2016MS000721.

Alo, C. A., and G. L. Wang (2010), Role of vegetation dynamics in regional climate predictions over western Africa, *Clim. Dyn.*, *35*, 907–922, doi:10.1007/s00383-010-0744-z.

Asseng, S., et al. (2013), Uncertainty in simulating wheat yields under climate change, *Nat. Clim. Change*, *3*, 827–832, doi:10.1038/nclimate1916.

Baidya Roy, S., and R. Avissar (2002), Impact of land use/land cover change on regional hydrometeorology in Amazonia, *J. Geophys. Res.*, *107*(D20), doi:10.1029/2000JD000266.

Batjes, N. H. (2002), A homogenized soil profile data set for global and regional environmental research (WISE, Version 1.1), *Rep. 2002/01*, Int. Soil Ref. and Inf. Cent., Wageningen, Netherlands.

Berg, A., N. de Noblet-Ducoudré, B. Sultan, M. Lengaigne, and M. Guimberteau (2013), Projections of climate change impacts on potential C4 crop productivity over tropical regions, *Agric. For. Meteorol.*, *170*, 89–102.

Boé, J., L. Terray, F. Habets, and E. Martin (2006), A simple statistical-dynamical downscaling scheme based on weather types and conditional resampling, *J. Geophys. Res.*, *111*, D23106, doi:10.1029/2005JD006889.

Bonan, G. B., and S. Levis (2006), Evaluating aspects of the community land and atmosphere model (CLM3 and CAM3) using a Dynamic Global Vegetation Model, *J. Clim.*, *19*(11), 2290–2301.

Bonan, G. B., S. Levis, S. Sitch, M. Vertenstein, and K. W. Oleson (2003), A dynamic global vegetation model for use with climate models: Concepts and description of simulated vegetation dynamics, *Global Change Biol.*, *9*(11), 1543–1566.

Boote, K. J., J. W. Jones, G. Hoogenboom, and N. B. Pickering (1998), The CROPGRO model for grain legumes, in *Understanding Options for Agricultural Production*, edited by G. Y. Tsuji, G. Hoogenboom, and P. K. Thornton, pp. 99–128, Kluwer, Dordrecht, Netherlands.

Burney, J., S. Davis, and D. Lobell (2010), Greenhouse gas mitigation by agricultural intensification, *Proc. Natl. Acad. Sci.*, *107*(26), 12,052–12,057, doi:10.1073/pnas.0914216107.

Collins, W. J., et al. (2011), Development and evaluation of an Earth-system model—HadGEM2, *Geosci. Model Dev. Discuss.*, *4*(2), 997–1062, doi:10.5194/gmdd-4-997-2011.

Cook, K. H., and E. K. Vizy (2013), Projected changes in East African rainy seasons, *J. Clim.*, *26*, 5931–5948, doi:10.1175/JCLI-D-12-00455.1.

Cox, P. M. (2001), Description of the TRIFFID dynamic global vegetation model, *Tech. Note 24*, Hadley Cent., U. K. Meteorol. Off., Bracknell, U. K.

Davies-Barnard, T., P. J. Valdes, J. S. Singarayer, and C. D. Jones (2014a), Climatic impacts of land-use change due to crop yield increases and a universal carbon tax from a scenario model*, *J. Clim.*, *27*, 1413–1424, doi:10.1175/JCLI-D-13-00154.1.

Davies-Barnard, T., P. J. Valdes, J. S. Singarayer, F. M. Pacifico, and C. D. Jones (2014b), Full effects of land use change in the representative concentration pathways, *Environ. Res. Lett.*, *9*, doi:10.1088/1748-9326/9/11/114014.

Delire, C., J. A. Foley, and S. Thompson (2004), Long-term internal variability in a coupled atmosphere-biosphere model, *J. Clim.*, *17*, 3947–3959.

Delire, C., N. De Noblet-Ducoudre, A. Sima, and I. Gouriand (2011), Vegetation dynamics enhancing long-term climate variability confirmed by two models, *J. Clim.*, *24*, 2238–2257, doi:10.1175/2010JCLI3664.1.

Dunne, J. P., et al. (2012), GFDL's ESM2 global coupled climate–Carbon Earth System Models. Part I: Physical formulation and baseline simulation characteristics, *J. Clim.*, *25*(19),6646–6665, doi:10.1175/jcli-d-11-00560.1.

Emanuel, K. A. (1991), A scheme for representing cumulus convection in large-scale models, *J. Atmos. Sci.*, *48*(21), 2313–2335.

Erfanian, A., G. L. Wang, M. Yu, and R. Anyah (2016), Multi-model ensemble simulations of present and future climates over West Africa: Impacts of vegetation Dynamics, *J. Adv. Model. Earth Syst.*, *8*, 1411–1431, doi:10.1002/2016MS000660.

FAO, IFPRI, and SAGE (2006), Agro-Maps: A global spatial database of agricultural land-use statistics aggregated by sub-national administrative districts, Rome. [Available at http://www.fao.org/landandwater/agll/agromaps/interactive/index.jsp.]

Feddema, J. J., K. W. Oleson, G. B. Bonan, L. O. Mearns, L. E. Buja, G. A. Meehl, and W. M. Washington (2005a), The importance of land cover change in simulating future climates, *Science*, *310*, 1674–1678.

Feddema, J. J., K. Oleson, G. Bonan, L. Mearns, W. Washington, G. Meehl, and D. Nychka (2005b), A comparison of a GCM response to historical anthropogenic land cover change and model sensitivity to uncertainty in present-day land cover representations, *Clim. Dyn.*, *25*, 581–609.

Gent, P. R., G. Danabasoglu, L. J. Donner, M. M. Holland, E. C. Hunke, S. R. Jayne, D. M. Lawrence, R. B. Neale, P. J. Rasch, and M. Vertenstein (2011), The community climate system model version 4, *J. Clim.*, *24*(19), 4973–4991.

Giorgi, F., et al. (2012), RegCM4: Model description and preliminary tests over multiple CORDEX domains, *Clim. Res.*, *52*, 7–29.

Grell, G. A., J. Dudhia, and D. R. Stauffer (1994), A description of the fifth generation Penn State/NCAR Mesoscale Model (MM5), *NCAR Tech. Note NCAR/TN-3801STR*, 138 pp., Natl. Cent. for Atmos. Res., Boulder, Colo.

Hagos, S., L. R. Leung, Y. Xue, A. Boone, F. de Sales, N. Neupane, M. Huang, and J. H. Yoon (2014), Assessment of uncertainties in the response of the African monsoon precipitation to land use change simulated by a regional model, *Clim. Dyn.*, *43*(9-10), 2765–2775.

Hoogenboom, G., et al. (2012), *Decision Support System for Agrotechnology Transfer (DSSAT) version 4.5* [CD-ROM], Univ. of Hawaii, Honolulu.

Holtslag, A. A. M., E. I. F. de Bruijn, and H. L. Pan (1990), A high resolution air mass transformation model for short-range weather forecasting, *Mon. Weather Rev.*, *118*, 1561–1575.

Hurtt, G. C., L. P. Chini, S. Frolking, R. A. Betts, J. Feddema, G. Fischer, and Y. P. Wang (2011), Harmonization of land-use scenarios for the period 1500–2100: 600 years of global gridded annual land-use transitions, wood harvest, and resulting secondary lands, *Clim. Change*, *109*(1-2), 117–161, doi:10.1007/s10584-011-0153-2.

IIASA/FAO, (2012), Global Agro-ecological Zones (GAEZ v3.0), IIASA, Laxenburg, Austria and FAO, Rome, Italy.
IPCC (2013), Climate Change 2013: The Physical Science Basis. Contribution of Working Group I to the Fifth Assessment Report of the Intergovernmental Panel on Climate Change, edited by T. F. Stocker et al., 1535 pp., Cambridge Univ. Press, Cambridge, U. K., doi:10.1017/CBO9781107415324.
Ji, Z. M., G. L. Wang, J. S. Pal, and M. Yu (2016), Potential climate effect of mineral aerosols over West Africa. Part I: Model validation and contemporary climate evaluation, *Clim. Dyn.*, *46*, 1223–1239, doi:10.1007/s00382-015-2641-y.
Ji, Z. M., G. L. Wang, M. Yu, and J. S. Pal (2017), Potential climate effect of mineral aerosols' over West Africa, Part II: Impact of aerosols and land use on future climate, *Clim. Dyn.*, doi:10.1007/s00382-015-2792-x, in press.
Jones, A. D., K. V. Calvin, W. D. Collins, and J. Edmonds (2015), Accounting for radiative forcing from albedo change in future global land-use scenarios, *Clim. Change*, *131*, 691–703.
Jones, J. W., G. Hoogenboom, C. H. Porter, K. J. Boote, W. D. Batchelor, L. A. Hunt, P. W. Wilkens, U. Singhe, A. J. Gijsman, and J. T. Ritchie (2003), DSSAT cropping system model, *Eur. J. Agron.*, *18*, 235–265.
Kiehl, J. T., J. J. Hack, G. B. Bonan, B. A. Boville, B. P. Briegleb, D. L. Williamson, and P. J. Rasch (1996), Description of the NCAR Community Climate Model (CCM3), *NCAR Tech. Note NCAR/TN-4201STR*, 152 pp., Natl. Cent. for Atmos. Res., Boulder, Colo.
Kucharik, C. J., J. A. Foley, and C. Delire (2000), Testing the performance of a Dynamic Global Ecosystem Model: Water balance, carbon balance, and vegetation structure, *Global Biogeochem. Cycles*, *14*(3), 795–825.
Lawrence, D., and K. Vandecar (2014), Effects of tropical deforestation on climate and agriculture, *Nat. Clim. Change*, *5*, 27–36.
Lawrence, P. J., and T. N. Chase (2007), Representing a new MODIS consistent land surface in the Community Land Model (CLM 3.0), *J. Geophys. Res.*, *112*, G01023, doi:10.1029/2006JG000168.
Lawrence, P. J., et al. (2011), Parameterization improvements and functional and structural advances in Version 4 of the Community Land Model, *J. Adv. Model. Earth Syst.*, *3*, M03001, doi:10.1029/2011MS00045.
Lobell, D. B., W. Schlenker, and J. Costa-Roberts (2011), Climate trends and global crop production since 1980, *Science*, *333*, 616–620.
Long, S. P., E. A. Ainsworth, A. D. B. Leakey, J. Nosberger, and D. R. Ort (2006), Food for thought: Lower-than-expected crop yield stimulation with rising CO_2 concentrations, *Science*, *312*, 1918–1921.
Meehl, G. A., et al. (2013), Climate change projections in CESM1(CAM5) compared to CCSM4, *J. Clim.*, *26*, 6287–6308.
Mendelsohn, R., W. D. Nordhaus, and D. Shaw (1994), The impact of global warming on agriculture: A Ricardian analysis, *Am. Econ. Rev.*, *84*, 753–771.
Monfreda, C., N. Ramankutty, and J. A. Foley (2008), Farming the planet: 2. Geographic distribution of crop areas, yields, physiological types, and NPP in the year 2000, *Global Biogeochem. Cycles*, *22*, GB1022, doi:10.1029/2007GB002947.
Moorcroft, P. R. (2003), Recent advances in ecosystem-atmosphere interactions: An ecological perspective, *Proc. Biol. Sci.*, *270*, 1215–1227.
Neale, R. B., et al. (2012), Description of the NCAR Community Atmosphere Model (CAM 5.0), *Rep. NCAR/TN-486+STR*, Natl. Cent. for Atmos. Res., Boulder, Colo.
Oleson, K., *et al.* (2013), Technical description of version 4.5 of the Community Land Model (CLM), *NCAR Tech. Note NCAR/TN-503+STR*, 420 pp., Natl. Cent. for Atmos. Res., Boulder, Colo., doi:10.5065/D6RR1W7M.
Pal, J. S., E. F. Small, and E. A. B. Eltahir (2000), Simulation of regional-scale water and energy budgets: Representation of subgrid cloud and precipitation processes with RegCM, *J. Geophys. Res.*, *105*(D24), 29,579–29,594.
Parker, D. C., S. M. Manson, M. A. Janssen, M. J. Hoffmann, P. Deadman, S. M. Manson, S. Hall (2002), Multi-agent systems for the simulation of land-use and land-cover change: A review, *Ann. Assoc. Am. Geogr.*, *93*, 314–337.
Potter, P., N. Ramankutty, E. Bennett, and S. Donner (2010), Characterizing the spatial patterns of global fertilizer application and manure production, *Earth Interact.*, *14*, 1–22.
Ramankutty, N., and J. A. Foley (1999), Estimating historical changes in global land cover: Croplands from 1700 to 1992, *Global Biogeochem. Cycle*, *13*(4), 997–1027.
Ramankutty, N., C. Delire, and P. Snyder (2006), Feedbacks between agriculture and climate: An illustration of the potential unintended consequences of human land use activities, *Global Planet. Change*, *54*, 79–93.
Ramankutty, N., A. T. Evan, C. Monfreda, and J. Foley (2008), Farming the planet: 1. Geographic distribution of global agricultural lands in the year 2000, *Global Biogeochem. Cycles*, *22*, GB1003, doi:10.1029/2007GB002952.
Ritchie, J. T., T. S. Griffin, and B. S. Johnson (1995), SUBSTOR: Functional model of potato growth, development, and yield, in *Modelling and Parameterization of the Soil–Plant–Atmosphere System: A Comparison of Potato Growth Models*, edited by P. Kabat et al., pp. 401–434, Wageningen Press, Wageningen, Netherlands.
Ritchie, J. T., U. Singh, D. C. Godwin, and W. T. Bowen (1998), Cereal growth, development and yield, in *Understanding Options for Agricultural Production*, edited by G. Y. Tsuji, G. Hoogenboom, and P. K. Thornton, pp. 79–98, Kluwer, Dordrecht, Netherlands.
Romero, C. C., G. Hoogenboom, G. A. Baigorria, J. Koo, A. J. Gijsman, and S. Wood (2012), Reanalysis of a global soil database for crop and environmental modeling, *Environ. Modell. Software*, *35*, 163–170.
Rosegrant, M., C. Ringler, and I. de Jong (2011), Irrigation: Tapping potential, *IFPRI Background Pap. 15*, Int. Food Policy Res. Inst., Washington, D. C.
Rosegrant, M. W. (2012), *International Model for Policy Analysis of Agricultural Commodities and Trade (IMPACT) Model Description*, Int. Food Policy Res. Inst., Washington, D. C.
Rosegrant, M. W., M. Agcaoili-Sombilla, and N. D. Perez (1995), Global food projections to 2020: Implications for investment, *2020 Discuss. Pap. 5*, Int. Food Policy Res. Inst., Washington, D. C.
Ruane, A. C., et al. (2013), Multi-factor impact analysis of agricultural production in Bangladesh with climate change, *Global Environ. Change*, *23*(1), 338–350.
Saini, R., G. L. Wang, M. Yu, and J. H. Kim (2015), Comparison of RCMs and GCMs projections of summer precipitation in West Africa, *J. Geophys. Res. Atmos.*, *120*, 3679–3699, doi:10.1002/2014JD022599.
Schaldach, R., J. Alcamo, J. Koch, C. Kolking, D. M. Lapola, J. Schungel, and J. A. Priess (2011), An integrated approach to modelling land-use change on continental and global scales, *Environ. Modell. Software*, *26*(8), 1041–1051.
Schlenker, W., and D. B. Lobell (2010), Robust negative impacts of climate change on African agriculture, *Environ. Res. Lett.*, *5*, 014010.
Schmitz, C., H. van Meijl, P. Kyle, G. C. Nelson, S. Fujimori, A. Gurgel, and H. Alin (2014), Land-use change trajectories up to 2050: Insights from a global agro-economic model comparison, *Agric. Econ.*, *45*(1), 69–84, doi:10.1111/agec.12090.
Sheffield, J., G. Goteti, and E. F. Wood (2006), Development of a 50-yr, high resolution global dataset of meteorological forcings for land surface modeling, *J. Clim.*, *13*, 3088–3111.

Sitch, S., et al. (2003), Evaluation of ecosystem dynamics, plant geography and terrestrial carbon cycling in the LPJ dynamic global vegetation model, *Global Change Biol.*, *9*, 161–185.

Solmon, F., F. Giorgi, and C. Liousse (2006), Aerosol modelling for regional climate studies: Application to anthropogenic particles and evaluation over a European/African domain, *Tellus, Ser. B*, *58*(1), 51–72.

Sultan, B., et al. (2013), Assessing climate change impacts on sorghum and millet yields in the Sudanian and Sahelian savannas of West Africa, *Environ. Res. Lett.*, *8*(1), 014040.

Svendsen, M., M. Ewing, and S. Msangi (2009), Watermarks: Indicators of irrigation sector performance in Africa. Africa Infrastructure Country Diagnostic project report, *Background Pap. 4*, Int. Food Policy Res. Inst., Washington, D. C.

Taylor, K. E., R. J. Stouffer, and G. A. Meehl (2012), An overview of CMIP5 and the experiment design, *Bull. Am. Meteorol. Soc.*, *93*, 485–498, doi:10.1175/BAMS-D-11-00094.1.

Tubiello, F. N., et al. (2007), Crop response to elevated CO_2 and world food supply, *Eur. J. Agron.*, *26*, 215–223.

Verburg, P. H., K. Kok, R. G. Pontius Jr., and A. Veldkamp (2006), Modeling land-use and land-cover change, in *Land-Use and Land-Cover Change*, pp. 117–135, Springer, Berlin.

Waha, K., C. Müller, and S. Rolinski (2013), Separate and combined effects of temperature and precipitation change on maize yields in sub-Saharan Africa for mid-to late-21st century, *Global Planet. Change*, *106*, 1–12.

Wang, G. L., E. A. B. Eltahir, J. A. Foley, D. Pollard, and S. Levis (2004), Decadal variability of rainfall in the Sahel: Results from the coupled GENESIS-IBIS atmosphere-biosphere model, *Clim. Dyn.*, *22*(6-7), 625–637, doi:10.1007/s00382-004-0411-3.

Wang, G. L, Y. Miao, J. S. Pal, M. Rui, G. B. Bonan, S. Levis, and P. E. Thornton (2015), On the development of a coupled regional climate-vegetation model RCM-CLM-CN-DV and its validation in Tropical Africa, *Clim. Dyn.*, *46*, 515–539, doi:10.1007/s00382-015-2596-z.

Wang, G. L., M. Yu., and Y. K. Xue (2016), Modeling the potential contribution of land cover changes to the Sahel drought using a regional climate model: Sensitivity to lateral boundary conditions and experimental approach, *Clim. Dyn.*, *47*, 3457–3477, doi:10.1007/s00382-015-2812-x.

Wang, J., R. L. Bras, and E. A. B. Eltahir (2000), The impact of observed deforestation on the mesoscale distribution of rainfall and clouds in Amazonia, *J. Hydrometeorol.*, *1*(3), 267–286.

Wang, J., F. Chagnon, E. Williams, A. K. Betts, N. O. Renno, L. A. T. Machado, G. Bisht, R. Knox, and R. L. Bras (2009), Impact of deforestation in the Amazon basin on cloud climatology, *Proc. Natl. Acad. Sci. U. S. A.*, *106*(10), 3670–3674.

Watanabe, S., et al. (2011), MIROC-ESM 2010: Model description and basic results of CMIP 5-20 c 3 m experiments, *Geosci. Model Dev.*, *4*(4), 845–872.

Wilby, R. L. (1998), Statistical downscaling of general circulation model output: A comparison of methods, *Water Resour. Res.*, *34*(11), 2995–3008.

Wint, G. R., and T. P. Robinson (2007), Gridded Livestock of the World, 132 pp., FAO, Rome.

Xie, H., L. You, B. Wielgosz, and C. Ringler (2014), Estimating the potential for expanding smallholder irrigation in Sub-Saharan Africa, *Agric. Water Manage.*, *131*(2014), 183–193.

Xue, Y., and J. Shukla (1993), The influence of land surface properties on Sahel climate. Part I: Desertification, *J. Clim.*, *6*, 2232–2246.

You, L., and S. Wood (2006), An entropy approach to spatial disaggregation of agricultural production, *Agric. Syst.*, *90*, 329–347, doi:10.1016/j.agsy.2006.01.008.

You, L., S. Wood, and U. Wood-Sichra (2009), Generating plausible crop distribution maps for Sub-Saharan Africa using a spatially disaggregated data fusion and optimization approach, *Agric. Syst.*, *99*, 126–140.

You, L., S. Wood, U. Wood-Sichra, and W. Wu (2014), Generating global crop distribution maps: From census to grid, *Agric. Syst.*, *127*(2014), 53–60.

Yu, M., G. L. Wang, D. T. Parr, and K. F. Ahmed (2014), Future changes of the terrestrial ecosystem based on a dynamic vegetation model driven with RCP8.5 climate projections from 19 GCMs, *Clim. Change*, *127*, 257–271, doi:10.1007/s10584-014-1249-2.

Yu, M., G. L. Wang, and J. S. Pal (2015), Impact of vegetation feedback on future climate change over West Africa, *Clim. Dyn.*, *46*, 3669–3688, doi:10.1007/s00382-015-2795-7.

Zakey, A. S., F. Solmon, and F. Giorgi (2006), Implementation and testing of a desert dust module in a regional climate model, *Atmos. Chem. Phys.*, *6*, 4687–4704, doi:10.5194/acp-6-4687-2006.

Zeng, N., J. D. Neelin, K.-M. Lau, and C. J. Tucker (1999), Enhancement of interdecadal climate variability in the Sahel by vegetation interaction, *Science*, *286*, 1537–1540, doi:10.1126/science.286.5444.1537.